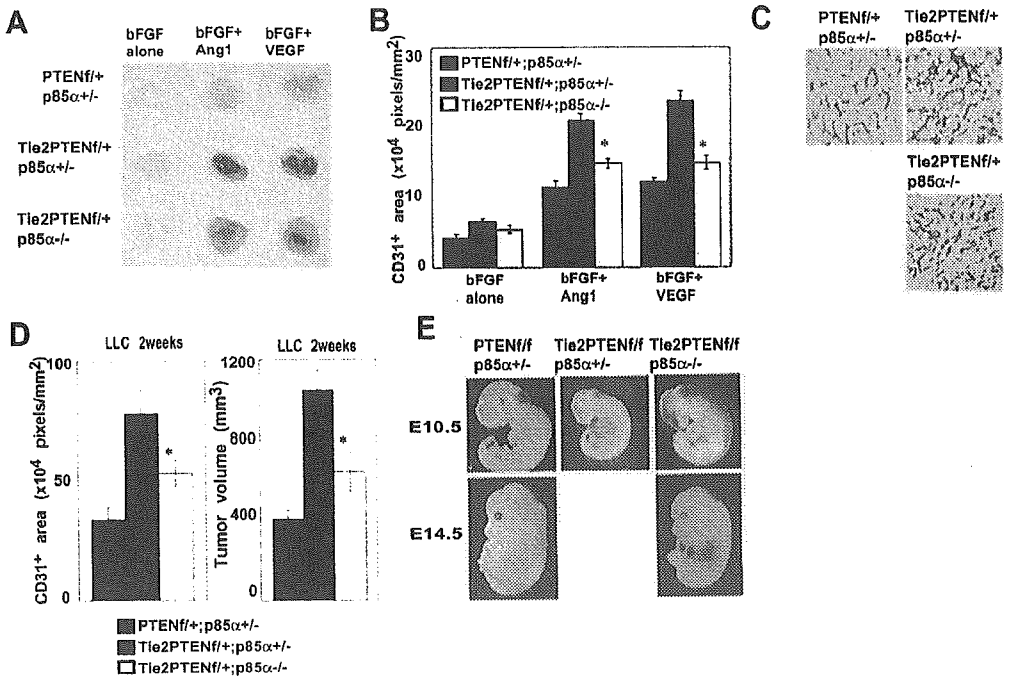

Figure 6. Partial rescue of Pten deficiency by *p85α* deficiency. (*A,B*) Mitigation of increased angiogenesis driven by VGFs in *p85α*$^{-/-}$*Tie2CrePten*$^{flox/+}$ mice. (*A*) Representative photos of Matrigel plugs containing *b*FGF, bFGF + Ang-1, or *b*FGF + VEGF-A. Plugs were removed from mice of the indicated genotypes at 14 d post-injection. (*B*) Quantitated vascularization of the Matrigel plugs in *A*. *p85α* deficiency significantly decreases the plug vascularization response (n = 5/genotype). (*C,D*) Mitigation of increased tumor growth and tumor angiogenesis. Shown are the results of anti-CD31 staining of sections of LLC tumors (*C*), quantitated tumor vascularization (*D, left*), and tumor growth (*D, right*) at 2 wk post-LLC inoculation (n = 4/genotype). Loss of *p85α* decreased the tumor vascularization and tumor volume observed in *Tie2CrePten*$^{flox/+}$ mice. (*E*) Whole mounts of E10.5 and E14.5 embryos of the indicated genotypes showed that loss of p85α partially restored the development of *Tie2CrePten*$^{flox/flox}$ embryos. However, due to extensive bleeding, these embryos did not survive beyond E14.5–E15.5. For *B* and *D*, quantitative results are expressed as the mean ± SEM and are representative of four trials. Statistical differences were determined using the Student's t-test; (*) $p < 0.05$.

β1 or its receptor show abnormal capillary structure due to defective angiogenesis possibly associated with impaired PC/vSMC differentiation (Dickson et al. 1995; Larsson et al. 2001). However, TGF-β1 was increased rather than decreased in our *Tie2CrePten*$^{flox/flox}$ mice. PKB/Akt activation inhibits Smad3, which eventually blocks TGF-β signaling (Remy et al. 2004). However, when we examined the expression of PAI-1, a downstream target molecule widely used to detect TGF-β activation, it was clear that such a mechanism was not operating in Pten-deficient endothelial cells at midgestation.

VEGF is a multifunctional VGF that stimulates the migration, proliferation, and survival of endothelial cells and promotes microvascular permeability and angiogenesis. VEGF also recruits PCs to the endothelial plexus (Benjamin et al. 1998). The expression of VEGF-A and its receptors was increased in *Tie2CrePten*$^{flox/flox}$ mice, consistent with a previous report in which activation of the PI3K pathway led to augmented VEGF-A expression (Jiang et al. 2000). Increased VEGF expression during lung organogenesis overstimulates endothelial cell growth and leads to abnormally large capillaries (Zeng et al. 1998). Mice overexpressing VEGF die at E14 due to cardiac abnormalities (Miquerol et al. 2000). We speculate that the Pten deficiency in our homozygous mutant mice contributed to increased VEGF signaling, leading to large capillary lumens with increased numbers of endothelial cells as well as a thin myocardium in the heart.

VCAM-1 signaling is also important for cardiovascular development, and VCAM-1 deficiency causes pericardial bleeding and impaired cardiomyocyte development (Kwee et al. 1995). The dramatic reduction of VCAM-1 expression in *Tie2CrePten*$^{flox/flox}$ embryos might partially explain their cardiac phenotypes. Defects in additional VGFs, their receptors, or cell adhesion molecules acting downstream of PI3K and PKB/Akt may also contribute to the cardiovascular defect.

Pten is deleted only in the endocardium and not in the myocardium of *Tie2CrePten*$^{flox/flox}$ mice. However, *Tie2CrePten*$^{flox/flox}$ mice showed a thin myocardial layer, in contrast to the well-developed trabecular folds observed in myocardium-specific Pten-deficient mice (Crackower et al. 2002). We speculate that this discrepancy arises because the abnormal endocardium of *Tie2CrePten*$^{flox/flox}$ mice cannot provide the appropriate inductive interactions for proper development of the underlying myocardium (Suri et al. 1996).

Mutation of p85α *or* p110γ *partially rescues endothelial cell-specific Pten defects*

The precise functions of PI3K isoforms in endothelial cells have been difficult to ascertain. Because most VGF receptors have tyrosine kinase activity, class IA PI3Ks likely play major roles in cardiovasculogenesis and tumor angiogenesis. Indeed, endothelial cell growth/survival and angiogenesis are enhanced following ectopic expression of constitutively active *p110α*, the catalytic subunit of class IA PI3Ks (Jiang et al. 2000). Consistent with this finding, the enhanced angiogenesis and accelerated tumor growth observed in our *Tie2CrePten*$^{flox/+}$ mice, and the impaired cardiovascular morphogenesis observed in our *Tie2CrePten*$^{flox/flox}$ mice were partially resolved by loss of *p85α*, the major regulatory subunit of class IA PI3Ks.

In this study, we shed light on the potential roles of the class IB PI3K in cardiovascular morphogenesis and post-natal angiogenesis. We generated double mutant mice lacking both Pten and class IB PI3K functions and demonstrated that the post-natal angiogenic responses of *Tie2CrePten*$^{flox/+}$ mice were rescued to the same degree by loss of *p110γ*, the catalytic subunit of PI3Kγ, as by loss of *p85α*. Furthermore, compared with *p85α deficiency*, *p110γ* deficiency dramatically resolved the defective cardiovasculogenesis observed in *Tie2CrePten*$^{flox/flox}$ mice. In the *p85α*-deficient mice used in this study, only the p85α isoform was deleted, not its alternative splicing isoforms p55α and p50α. Moreover, *p85β* and *p55γ*, the alternative regulatory subunits of class IA PI3Ks, still exist in these mice. However, since *p85α* is the major regulatory subunit of class IA PI3Ks, we believe that the class IB PI3K may have a more important function in cardiovasculogenesis than do the class IA PI3Ks.

We did not expect the enhanced angiogenesis induced in *Tie2CrePten*$^{flox/+}$ mice by RTK agonists (e.g., VEGF and Ang-1) to be partially rescued by *p110γ* deficiency. Up until now, *p110γ* has been postulated to be activated downstream of GPCR but not downstream of RTK. Indeed, the activation of PKB/Akt and MAPK induced by VEGF and Ang-1 was not suppressed by *p110γ* deficiency in vitro (Supplementary Fig. 4A). It is thus unlikely that an RTK type VGF receptor directly couples with p110γ, an interaction noted for PDGF receptors and erythropoietin receptors (Kaplan-Albuquerque et al. 2003). It may be that, in vivo, an unknown VGF (possibly a GPCR ligand) activates p110γ and influences RTK signaling that is initiated by VEGF or Ang-1 and leads to angiogenesis. In endothelial cells, identified GPCR ligands include sphingosine-1-phosphate (S1P), angiotensin II, CXCL-16, and shear stress (Stoyanov et al. 1995; Dimmeler et al. 1998). One of the candidate GPCR ligands that may activate p110γ in endothelial cells is S1P. S1P induces endothelial cell proliferation, migration, and morphogenesis in vitro and in vivo (Lee et al. 1999). Moreover, EDG1, a GPCR-type S1P receptor, is essential for vascular maturation (Liu et al. 2000). We have shown here that *p110γ* deficiency partially blocks enhanced angiogenesis driven not only by Ang-1 or VEGF-A but also by S1P (Supplementary Fig. 4B). However, S1P-induced activation of PKB/Akt and MAPK was not suppressed by *p110γ* deficiency (Supplementary Fig. 4A), indicating that the major downstream target of S1P may not be *p110γ*.

Although PTEN has dual lipid and protein phosphatase activities (Maehama and Dixon 1998; Li and Sun 1997), our results clearly demonstrate that a primary function of PTEN is to fine-tune the intracellular level of PIP3 produced by PI3Ks and thereby regulate vascular remodeling and tumor angiogenesis. Our data also suggest the functional overlapping of class IA and IB PI3Ks in angiogenesis. This hypothesis is supported by the lack of an endothelial cell phenotype in mice lacking *p85α* (Fruman et al. 1999; Terauchi et al. 1999), *p85β* (Ueki et al. 2002), *p110β* (Bi et al. 2002), or *p110γ* (Sasaki et al. 2000) or in *p110δ* "kinase dead" knock-in mice (Okkenhaug et al. 2002). Furthermore, our results demonstrate that, among the multiple PIP3 phosphatases, PTEN has an exclusive role in down-regulating PIP3 in endothelial cells. Various PI3Kγ-specific inhibitors that are under investigation as anti-inflammatory drugs may therefore also be useful as cancer therapies targeting tumor angiogenesis.

Our study is the first report of the functional analysis of Pten and PI3Kγ in murine endothelial cells in vivo. We have demonstrated that the normal function of the PI3K–PKB/Akt–Pten pathway in endothelial cells is required for cardiovascular development, and that loss of Pten-mediated control of this pathway enhances tumor angiogenesis. Deficiency in Pten function thus contributes both to susceptibility to new tumorigenic mutations and to accelerated tumor growth. Inhibition of the PI3K pathway, including PI3Kγ, is thus an attractive therapeutic target for the treatment of various malignancies.

Materials and methods

Generation of mutant mice

Pten$^{flox/flox}$ mice (C57BL6/J background), generated as previously described (Suzuki et al. 2001), were mated to *Tie2Cre* transgenic mice (C57BL6/J background) (Koni et al. 2001), in which expression of Cre is controlled by the *Tie2* promoter. *Tie2* is strongly activated in endothelial cells. Male *Pten*$^{flox/flox}$ mice were crossed with female *Tie2CrePten*$^{flox/+}$ mice to avoid the ectopic recombination observed when the *Tie2Cre* locus is transmitted from male mice. Offspring carrying *Tie2Cre* and two copies of the floxed *Pten* allele (*Tie2CrePten*$^{flox/flox}$), *Tie2Cre* plus one copy of the floxed *Pten* allele (*Tie2CrePten*$^{flox/+}$), and *Tie2Cre* plus two copies of the wild-type *Pten* allele (*Tie2CrePten*$^{+/+}$) were used in analyses as homozygous mutant (*Tie2CrePten*$^{flox/flox}$), heterozygous mutant (*Tie2CrePten*$^{flox/+}$), and wild-type (*Tie2CrePten*$^{+/+}$) mice, respectively. *p110γ*$^{-/-}$*Tie2CrePten*$^{flox/flox}$ and *p85α*$^{-/-}$*Tie2CrePten*$^{flox/flox}$ double mutant mice were generated by crossing male *p110γ*$^{-/-}$ (C57BL6/J background) (Sasaki et al. 2000) or *p85α*$^{-/-}$ mice (C57BL6/J background) (Terauchi et al. 1999) with female *Tie2CrePten*$^{flox/+}$ mice, followed by the crossing of male *p110γ*$^{-/-}$*Pten*$^{flox/flox}$ or *p85α*$^{-/-}$*Pten*$^{flox/flox}$ mice with female *p110γ* $^{+/-}$*Tie2CrePten*$^{flox/+}$ or *p85α* $^{+/-}$*Tie2CrePten*$^{flox/+}$ mice, respectively.

Homologous recombination was detected using a GFP reporter gene as described previously (Kawamoto et al. 2000). Briefly, the reporter transgene contains the CAG promoter, the loxP-flanked CAT gene with an SV40 polyadenylation signal, and the GFP gene at the 3′ end (STOP^{flox}-GFP). Mice carrying both the *Tie2Cre* and *STOP^{flox}-GFP* transgenes were generated to identify cells in which recombination had occurred. *Flk-LacZ* knock-in mutant mice have been described previously (Yamaguchi et al. 1993). Interbreeding of *Tie2CrePten$^{flox/+}$* and *Flk-LacZ* heterozygous mutant mice generated *Pten* homozygous and *Flk-LacZ* heterozygous double mutant mice. Littermate embryos were used for all experiments. The Institutional Review Board of the Akita University School of Medicine approved all animal experiments.

PCR analysis of Pten genotypes

Genomic DNA from mouse tails was isolated and amplified by PCR as described (Suzuki et al. 2001). Sequences of sense and anti-sense primers for floxed and wild-type *Pten* alleles and the *Tie2Cre* transgene are listed in Supplementary Table 1. Amplified fragments of 705 bp (Δ *Pten*), 514 bp (floxed *Pten*), 428 bp (wild-type *Pten*), and 269 bp (*Tie2Cre* transgene) were obtained.

RT–PCR

To assay VGF expression, RNA from 10^4 cells was extracted using an RNeasy Mini kit (Qiagen, Inc.) and reverse transcribed using an Advantage RT-for-PCR Kit (Clontech). Sequences of specific primers and amplified product sizes are listed in Supplementary Table 1.

Matrigel plug assays

Matrigel plug assays were performed as described previously (Prewett et al. 1999). Six-week-old mice were injected subcutaneously at the abdominal midline with 0.5 mL Matrigel (BD Biosciences) supplemented with 250 ng *b*FGF (R&D Systems) and/or 5 ng VEGF-A (VEGF165; PeproTech EC Ltd.) and/or 150 ng Ang-1 (provided by G.Y. Koh, KAIST, Deajeon, Korea). Control mice were injected with PBS-Matrigel. Mice were sacrificed 14 d after Matrigel injection, and vascularization was quantitated by immunohistological examination using anti-PECAM-1/CD31 antibody (Pharmingen) and a horseradish peroxidase-conjugated anti-rat Ig secondary antibody (Biosource International). Samples were then incubated with PBS containing 0.3 mg/mL diaminobenzidine (Dojin Laboratories) in the presence of 0.05% $NiCl_2$ for 10–30 min at room temperature, followed by the addition of 0.01% hydrogen peroxide. Infiltration of capillaries into the Matrigel was visualized by anti-CD31 staining and quantitated using NIH image software.

Tumor formation assay

The tumorigenicity of murine LLC cells or B16-BL6 melanoma cells was assayed by injecting 2×10^5 cells subcutaneously into the backs of 8-wk-old *Tie2CrePten$^{+/+}$* and *Tie2CrePten$^{flox/+}$* mice. After 14 d (LCC) or 21 d (B16-BL6), tumor diameters were measured using calipers. Tumor diameter was converted to tumor volume using the calculation: volume = $4/3\pi r^3$.

Isolation of MLECs

MLECs of *Tie2CrePten$^{+/+}$* and *Tie2CrePten$^{flox/+}$* mice were prepared as previously described (Hartwell et al. 1998). Briefly, lung tissues were excised, digested with 0.1% collagenase A (Sigma), and disaggregated by nylon-mesh to produce a single suspension. This mixed population was negatively selected with anti-CD16 mAb (Pharmingen), positively selected with anti-ICAM-2 mAb (Pharmingen), and purified using anti-IgG-coated magnetic beads (Dynal Biotech). The endothelial cell population was >90% pure as assessed by anti-CD31 staining. MLECs were grown on a 1% gelatin-coated dish in Ham's F-12 medium supplemented with 20% FBS, 0.2 U/mL heparin, and endothelial mitogen (Biomedical Technologies) (Hartwell et al. 1998).

Cell proliferation and transmigration assays

Cell proliferation in response to 24 h stimulation with Ang-1 (300 ng/mL) or VEGF-A (10 ng/mL) was evaluated by PCNA immunostaining as previously described (Zhang et al. 2004). Cell transmigration assays were performed as described (Ito et al. 2003) using MLECs from 8–10-wk-old *Tie2CrePten$^{+/+}$* and *Tie2CrePten$^{flox/+}$* mice. Migration was measured 4 h after the addition of Ang-1 (300 ng/mL) or VEGF-A (10 ng/mL) to the lower chamber of a Transwell.

Whole-mount embryo immunostaining and LacZ staining

Immunostaining was conducted using anti-CD31 antibody or anti-smooth muscle actin antibody (1A4; Dako Cytomation). For LacZ staining, embryos and yolk sacs were fixed in cold 4% paraformaldehyde in PBS for 10 min, rinsed twice with PBS, and stained from 2 h to overnight at 37°C in X-Gal buffer (5 mM potassium ferrocyanide, 5 mM potassium ferricyanide, 2 mM $MgCl_2$, and 1 mg/mL X-Gal in PBS at pH 7.2).

Electron microscopy

The placentae and yolk sacs of E9.5 embryos were isolated, washed with washing buffer (3.5% sucrose in 0.1 M sodium cacodylate buffer at pH 7.3), post-fixed in buffered osmium tetroxide, and embedded in epoxy according to standard procedures. Ultrathin sections were stained in uranyl acetate and lead citrate and examined using a 100CX electron microscope operated at 60 kV (JEOL)

Cell culture and siRNA transfection

Primary HUVECs (Clonetics Corp.) were grown in the EGM-2 Bullet kit (Clonetics) containing FBS and supplemental growth factors. HUVECs (5×10^4 cells/well) were cultured in 24-well plates, and transfections were performed using Lipofectamine 2000 (Invitrogen) according to the manufacturer's protocol. Lipofectamine 2000 (2 μL) and 0.2 μg siRNA was used for each transfection. Sequences of siRNAs corresponded to nucleotides 1081–1105 or 1053–1077 of human PTEN (GenBank accession no. NM 000314) or were mismatched siRNAs: PTENsiRNA#1, 5′-AAGAGGAUGGAUUCGACUUAGACUU-3′; PTENsiRNA#2, 5′-AUCGUUAGCAGAAACAAAAGGAGAU-3′; control mismatch siRNA#1, 5′-AAGAGGAUGGUAUCGACUUAGACUU-3′; and control mismatch siRNA#2, 5′-AUCGUGAGCACAAA GAAAAUGAGAU-3′. RNA duplexes (25 nucleotides) with AG overhangs (sense) and AU overhangs (anti-sense) at both 3′-ends were prepared as described (Miyagishi and Taira 2002).

Western blotting

Total cell lysates (30 μg) were analyzed by Western blotting using the following antibodies: anti-human PTEN (Cascade Bioscience); antibodies against connexin 40, Ang-1, Ang-2, VEGF-A, TGF-β, ephrinB2, VCAM-1, or actin (all from Santa Cruz Biotechnology); anti-VEGFR1 (R&D Systems); and anti-VEGFR2 (Kyowa Hakko). For assays involving *Tie2CrePten$^{flox/+}$* MLECs, VEGF-A (10 ng/mL) was added for 24 h prior to lysate preparation.

Flow cytometric analysis

HUVECs were preincubated with anti-CD16 mAb to minimize nonspecific staining. Cells were then stained with PE-conjugated anti-VEGFR1 (R&D Systems) or anti-VEGFR2 (Kyowa Hakko), followed by FITC-conjugated anti-mouse IgG (Becton Dickinson). Flow cytometric analysis was performed using a FACSCalibur with CELLQuest software (Becton Dickinson).

Acknowledgments

We thank Dr. Shigeo Koyasu and Dr. Yuichi Oike (Keio University); Dr. Tetsuo Noda and Dr. Noriko Ohsumi (Tohoku University); Dr. Shin Yonehara (Kyoto University); Dr. Nobuyuki Takakura (Kanazawa University); and Dr. Shunsuke Takasuga, Ms. Motoka Yamada, Ms. Naoko Baba, Ms. Yuki Sakamoto, and Mr. Akihiko Tomita (Akita University) for helpful discussions and technical support. We also thank Dr. Shigeo Koyasu (Keio University), Dr. Janet Rossant (Samuel Lunenfeld Research Institute, Toronto), and Dr. Irmgard Forster (Institute for Medical Microbiology, Immunology, and Hygiene, Munich) for providing the *p85α*$^{-/-}$, *Flk-LacZ* knock-in mutant mice, and LysMCre transgenic mice, respectively. This work was supported by grants from the Ministry of Education, Science, Sports and Culture, Japan; the Daiwa Securities Health Foundation; the Osaka Cancer Research Foundation; the Japanese Heart Foundation; the Takeda Science Foundation; the Uehara Memorial Foundation; and the Yamanouchi Foundation for Research on Metabolic Disorders.

References

Antonelli-Orlidge, A., Saunders, K.B., Smith, S.R., and D'Amore, P.A. 1989. An activated form of transforming growth factor β is produced by cocultures of endothelial cells and pericytes. *Proc. Natl. Acad. Sci.* **86:** 4544–4548.

Benjamin, L.E., Hemo, I., and Keshet, E. 1998. A plasticity window for blood vessel remodelling is defined by pericyte coverage of the preformed endothelial network and is regulated by PDGF-B and VEGF. *Development* **125:** 1591–1598.

Bi, L., Okabe, I., Bernard, D.J., and Nussbaum, R.L. 2002. Early embryonic lethality in mice deficient in the p110β catalytic subunit of PI 3-kinase. *Mamm. Genome* **13:** 169–172.

Bingle, L., Brown, N.J., and Lewis, C.E. 2002. The role of tumour-associated macrophages in tumour progression: Implications for new anticancer therapies. *J. Pathol.* **196:** 254–265.

Crackower, M.A., Oudit, G.Y., Kozieradzki, I., Sarao, R., Sun, H., Sasaki, T., Hirsch, E., Suzuki, A., Shioi, T., Irie-Sasaki, J., et al. 2002. Regulation of myocardial contractility and cell size by distinct PI3K–PTEN signaling pathways. *Cell* **110:** 737–749.

Daniel, T.O. and Abrahamson, D. 2000. Endothelial signal integration in vascular assembly. *Annu. Rev. Physiol.* **62:** 649–671.

Dickson, M.C., Martin, J.S., Cousins, F.M., Kulkarni, A.B., Karlsson, S., and Akhurst, R.J. 1995. Defective haematopoiesis and vasculogenesis in transforming growth factor-β 1 knock out mice. *Development* **121:** 1845–1854.

Dimmeler, S., Assmus, B., Hermann, C., Haendeler, J., and Zeiherk, A.M. 1998. Fluid shear stress stimulates phosphorylation of Akt in human endothelial cells: Involvement in suppression of apoptosis. *Circ. Res.* **83:** 334–341.

Dumont, D.J., Gradwohl, G., Fong, G.H., Puri, M.C., Gertsenstein, M., Auerbach, A., and Breitman, M.L. 1994. Dominant-negative and targeted null mutations in the endothelial receptor tyrosine kinase, tek, reveal a critical role in vasculogenesis of the embryo. *Genes & Dev.* **8:** 1897–1909.

Folkman, J. and Shing, Y. 1992. Angiogenesis. *J. Biol. Chem.* **267:** 10931–10934.

Fruman, D.A., Snapper, S.B., Yballe, C.M., Davidson, L., Yu, J.Y., Alt, F.W., and Cantley, L.C. 1999. Impaired B cell development and proliferation in absence of phosphoinositide 3-kinase p85α. *Science* **283:** 393–397.

Furuyama, T., Kitayama, K., Shimoda, Y., Ogawa, M., Sone, K., Yoshida-Araki, K., Hisatsune, H., Nishikawa, S., Nakayama, K., Ikeda, K., et al. 2004. Abnormal angiogenesis in Foxo1 (Fkhr)-deficient mice. *J. Biol. Chem.* **279:** 34741–34749.

Gerber, H.P., McMurtrey, A., Kowalski, J., Yan, M., Keyt, B.A., Dixit, V., and Ferrara, N. 1998. Vascular endothelial growth factor regulates endothelial cell survival through the phosphatidylinositol 3′-kinase/Akt signal transduction pathway: Requirement for Flk-1/KDR activation. *J. Biol. Chem.* **273:** 30336–30343.

Hammes, H.P., Lin, J., Wagner, P., Feng, Y., Vom Hagen, F., Krzizok, T., Renner, O., Breier, G., Brownlee, M., and Deutsch, U. 2004. Angiopoietin-2 causes pericyte dropout in the normal retina: Evidence for involvement in diabetic retinopathy. *Diabetes* **53:** 1104–1110.

Hartwell, D.W., Mayadas, T.N., Berger, G., Frenette, P.S., Rayburn, H., Hynes, R.O., and Wagner, D.D. 1998. Role of P-selectin cytoplasmic domain in granular targeting in vivo and in early inflammatory responses. *J. Cell Biol.* **143:** 1129–1141.

Hellstrom, M., Gerhardt, H., Kalen, M., Li, X., Eriksson, U., Wolburg, H., and Betsholtz, C. 2001. Lack of pericytes leads to endothelial hyperplasia and abnormal vascular morphogenesis. *J. Cell Biol.* **153:** 543–553.

Huang, J. and Kontos, C.D. 2002. PTEN modulates vascular endothelial growth factor-mediated signaling and angiogenic effects. *J. Biol. Chem.* **277:** 10760–10766.

Hungerford, J.E. and Little, C.D. 1999. Developmental biology of the vascular smooth muscle cell: Building a multilayered vessel wall. *J. Vasc. Res.* **36:** 2–27.

Ito, Y., Oike, Y., Yasunaga, K., Hamada, K., Miyata, K., Matsumoto, S., Sugano, S., Tanihara, H., Masuho, Y., and Suda, T. 2003. Inhibition of angiogenesis and vascular leakiness by angiopoietin-related protein 4. *Cancer Res.* **63:** 6651–6657.

Jain, R.K. 2003. Molecular regulation of vessel maturation. *Nat. Med.* **9:** 685–693.

Jiang, B.H., Zheng, J.Z., Aoki, M., and Vogt, P.K. 2000. Phosphatidylinositol 3-kinase signaling mediates angiogenesis and expression of vascular endothelial growth factor in endothelial cells. *Proc. Natl. Acad. Sci.* **97:** 1749–1753.

Kaplan-Albuquerque, N., Garat, C., Desseva, C., Jones, P.L., and Nemenoff, R.A. 2003. Platelet-derived growth factor-BB-mediated activation of Akt suppresses smooth muscle-specific gene expression through inhibition of mitogen-activated protein kinase and redistribution of serum response factor. *J. Biol. Chem.* **278:** 39830–39838.

Kawamoto, S., Niwa, H., Tashiro, F., Sano, S., Kondoh, G., Takeda, J., Tabayashi, K., and Miyazaki, J. 2000. A novel reporter mouse strain that expresses enhanced green fluorescent protein upon Cre-mediated recombination. *FEBS Lett.* **470:** 263–268.

Kim, K.J., Li, B., Winer, J., Armanini, M., Gillett, N., Phillips, H.S., and Ferrara, N. 1993. Inhibition of vascular endothelial growth factor-induced angiogenesis suppresses tumour growth in vivo. *Nature* **362:** 841–844.

Koni, P.A., Joshi, S.K., Temann, U.A., Olson, D., Burkly, L., and Flavell, R.A. 2001. Conditional vascular cell adhesion molecule 1 deletion in mice: Impaired lymphocyte migration to bone marrow. *J. Exp. Med.* **193:** 741–754.

Kwee, L., Baldwin, H.S., Shen, H.M., Stewart, C.L., Buck, C., Buck, C.A., and Labow, M.A. 1995. Defective development of the embryonic and extraembryonic circulatory systems in

vascular cell adhesion molecule (VCAM-1) deficient mice. *Development* **121:** 489–503.

Larsson, J., Goumans, M.J., Sjostrand, L.J., van Rooijen, M.A., Ward, D., Leveen, P., Xu, X., ten Dijke, P., Mummery, C.L., and Karlsson, S. 2001. Abnormal angiogenesis but intact hematopoietic potential in TGF-β type I receptor-deficient mice. *EMBO J.* **20:** 1663–1673.

Lee, M.J., Thangada, S., Claffey, K.P., Ancellin, N., Liu, C.H., Kluk, M., Volpi, M., Sha'afi, R.I., and Hla, T. 1999. Vascular endothelial cell adherens junction assembly and morphogenesis induced by sphingosine-1-phosphate. *Cell* **99:** 301–312.

Li, D.M. and Sun, H. 1997. TEP1, encoded by a candidate tumor suppressor locus, is a novel protein tyrosine phosphatase regulated by transforming growth factor β. *Cancer Res.* **57:** 2124–2129.

Li, J., Yen, C., Liaw, D., Podsypanina, K., Bose, S., Wang, S.I., Puc, J., Miliaresis, C., Rodgers, L., McCombie, R., et al. 1997. PTEN: A putative protein tyrosine phosphatase gene mutated in human brain, breast, and prostate cancer. *Science* **275:** 1943–1947.

Liaw, D., Marsh, D.J., Li, J., Dahia, P.L., Wang, S.I., Zheng, Z., Bose, S., Call, K.M., Tsou, H.C., Peacocke, M., et al. 1997. Germline mutations of the PTEN gene in Cowden disease: An inherited breast and thyroid cancer syndrome. *Nat. Genet.* **16:** 64–67.

Lindahl, P., Johansson, B.R., Leveen, P., and Betsholtz, C. 1997. Pericyte loss and microaneurysm formation in PDGF-B-deficient mice. *Science* **277:** 242–245.

Lindblom, P., Gerhardt, H., Liebner, S., Abramsson, A., Enge, M., Hellstrom, M., Backstrom, G., Fredriksson, S., Landegren, U., Nystrom, H.C., et al. 2003. Endothelial PDGF-B retention is required for proper investment of pericytes in the microvessel wall. *Genes & Dev.* **17:** 1835–1840.

Liu, Y., Wada, R., Yamashita, T., Mi, Y., Deng, C.X., Hobson, J.P., Rosenfeldt, H.M., Nava, V.E., Chae, S.S., Lee, M.J., et al. 2000. Edg-1, the G protein-coupled receptor for sphingosine-1-phosphate, is essential for vascular maturation. *J. Clin. Invest.* **106:** 951–961.

Maehama, T. and Dixon, J.E. 1998. The tumor suppressor, PTEN/MMAC1, dephosphorylates the lipid second messenger, phosphatidylinositol 3,4,5-trisphosphate. *J. Biol. Chem.* **273:** 13375–13378.

Maisonpierre, P.C., Suri, C., Jones, P.F., Bartunkova, S., Wiegand, S.J., Radziejewski, C., Compton, D., McClain, J., Aldrich, T.H., Papadopoulos, N., et al. 1997. Angiopoietin-2, a natural antagonist for Tie2 that disrupts in vivo angiogenesis. *Science* **277:** 55–60.

Miquerol, L., Langille, B.L., and Nagy, A. 2000. Embryonic development is disrupted by modest increases in vascular endothelial growth factor gene expression. *Development* **127:** 3941–3946.

Miyagishi, M. and Taira, K. 2002. U6 promoter-driven siRNAs with four uridine 3′ overhangs efficiently suppress targeted gene expression in mammalian cells. *Nat. Biotechnol.* **20:** 497–500.

Morales-Ruiz, M., Lee, M.J., Zollner, S., Gratton, J.P., Scotland, R., Shiojima, I., Walsh, K., Hla, T., and Sessa, W.C. 2001. Sphingosine 1-phosphate activates Akt, nitric oxide production, and chemotaxis through a Gi protein/phosphoinositide 3-kinase pathway in endothelial cells. *J. Biol. Chem.* **276:** 19672–19677.

Okkenhaug, K., Bilancio, A., Farjot, G., Priddle, H., Sancho, S., Peskett, E., Pearce, W., Meek, S.E., Salpekar, A., Waterfield, M.D., et al. 2002. Impaired B and T cell antigen receptor signaling in p110Δ PI 3-kinase mutant mice. *Science* **297:** 1031–1034.

Plate, K.H., Breier, G., and Risau, W. 1994. Molecular mechanisms of developmental and tumor angiogenesis. *Brain Pathol.* **4:** 207–218.

Prewett, M., Huber, J., Li, Y., Santiago, A., O'Connor, W., King, K., Overholser, J., Hooper, A., Pytowski, B., Witte, L., et al. 1999. Antivascular endothelial growth factor receptor (fetal liver kinase 1) monoclonal antibody inhibits tumor angiogenesis and growth of several mouse and human tumors. *Cancer Res.* **59:** 5209–5218.

Remy, I., Montmarquette, A., and Michnick, S.W. 2004. PKB/Akt modulates TGF-β signalling through a direct interaction with Smad3. *Nat. Cell Biol.* **6:** 358–365.

Sasaki, T., Irie-Sasaki, J., Jones, R.G., Oliveira-dos-Santos, A.J., Stanford, W.L., Bolon, B., Wakeham, A., Itie, A., Bouchard, D., Kozieradzki, I., et al. 2000. Function of PI3Kgamma in thymocyte development, T cell activation, and neutrophil migration. *Science* **287:** 1040–1046.

Shiojima, I. and Walsh, K. 2002. Role of Akt signaling in vascular homeostasis and angiogenesis. *Circ. Res.* **90:** 1243–1250.

Stoyanov, B., Volinia, S., Hanck, T., Rubio, I., Loubtchenkov, M., Malek, D., Stoyanova, S., Vanhaesebroeck, B., Dhand, R., Nurnberg, B., et al. 1995. Cloning and characterization of a G protein-activated human phosphoinositide-3 kinase. *Science* **269:** 690–693.

Su, J.D., Mayo, L.D., Donner, D.B., and Durden, D.L. 2003. PTEN and phosphatidylinositol 3′-kinase inhibitors upregulate p53 and block tumor-induced angiogenesis: Evidence for an effect on the tumor and endothelial compartment. *Cancer Res.* **63:** 3585–3592.

Sun, J.F., Phung, T., Shiojima, I., Felske, T., Upalakalin, J.N., Feng, D., Kornaga, T., Dor, T., Dvorak, A.M., Walsh, K., et al. 2005. Microvascular patterning is controlled by fine-tuning the Akt signal. *Proc. Natl. Acad. Sci.* **102:** 128–133.

Suri, C., Jones, P.F., Patan, S., Bartunkova, S., Maisonpierre, P.C., Davis, S., Sato, T.N., and Yancopoulos, G.D. 1996. Requisite role of angiopoietin-1: A ligand for the TIE2 receptor, during embryonic angiogenesis. *Cell* **87:** 1171–1180.

Suzuki, A., Yamaguchi, M.T., Ohteki, T., Sasaki, T., Kaisho, T., Kimura, Y., Yoshida, R., Wakeham, A., Higuchi, T., Fukumoto, M., et al. 2001. T cell-specific loss of Pten leads to defects in central and peripheral tolerance. *Immunity* **14:** 523–534.

Terauchi, Y., Tsuji, Y., Satoh, S., Minoura, H., Murakami, K., Okuno, A., Inukai, K., Asano, T., Kaburagi, Y., Ueki, K., et al. 1999. Increased insulin sensitivity and hypoglycaemia in mice lacking the p85 α subunit of phosphoinositide 3-kinase. *Nat. Genet.* **21:** 230–235.

Ueki, K., Yballe, C.M., Brachmann, S.M., Vicent, D., Watt, J.M., Kahn, C.R., and Cantley, L.C. 2002. Increased insulin sensitivity in mice lacking p85β subunit of phosphoinositide 3-kinase. *Proc. Natl. Acad. Sci.* **99:** 419–424.

Wang, H.U., Chen, Z.F., and Anderson, D.J. 1998. Molecular distinction and angiogenic interaction between embryonic arteries and veins revealed by ephrin-B2 and its receptor Eph-B4. *Cell* **93:** 741–753.

Yamaguchi, T.P., Dumont, D.J., Conlon, R.A., Breitman, M.L., and Rossant, J. 1993. flk-1, an flt-related receptor tyrosine kinase, is an early marker for endothelial cell precursors. *Development* **118:** 489–498.

Zeng, X., Wert, S.E., Federici, R., Peters, K.G., and Whitsett, J.A. 1998. VEGF enhances pulmonary vasculogenesis and disrupts lung morphogenesis in vivo. *Dev. Dyn.* **211:** 215–227.

Zhang, T., Chen, X., Qu, L., Wu, J., Cui, R., and Zhao, Y. 2004. Chrysin and its phosphate ester inhibit cell proliferation and induce apoptosis in Hela cells. *Bioorg. Med. Chem.* **12:** 6097–6105.

Role of p38 Mitogen-Activated Protein Kinase Activation in Podocyte Injury and Proteinuria in Experimental Nephrotic Syndrome

Masao Koshikawa,* Masashi Mukoyama,* Kiyoshi Mori,* Takayoshi Suganami,* Kazutomo Sawai,* Tetsuro Yoshioka,* Tetsuya Nagae,* Hideki Yokoi,* Hiroshi Kawachi,† Fujio Shimizu,† Akira Sugawara,* and Kazuwa Nakao*

**Department of Medicine and Clinical Science, Kyoto University Graduate School of Medicine, Kyoto, and †Department of Cell Biology, Institute of Nephrology, Niigata University Graduate School of Medical and Dental Sciences, Niigata, Japan*

Podocytes play an important role in maintaining normal glomerular function and structure, and podocyte injury leads to proteinuria and glomerulosclerosis. The family of mitogen-activated protein kinases (MAPK; extracellular signal-regulated kinase [ERK], c-Jun N-terminal kinase, and p38) may be implicated in the progression of various glomerulopathies, but the role of MAPK in podocyte injury remains elusive. This study examined phosphorylation of p38 MAPK in clinical glomerulopathies with podocyte injury, as well as in rat puromycin aminonucleoside (PAN) nephropathy and mouse adriamycin (ADR) nephropathy. The effect of treatment with FR167653, an inhibitor of p38 MAPK, was also investigated in rodent models. In human podocyte injury diseases, the increased phosphorylation of p38 MAPK was observed at podocytes. In PAN and ADR nephropathy, the phosphorylation of p38 MAPK and ERK was marked but transient, preceding overt proteinuria. Pretreatment with FR167653 (day −2 to day 14, subcutaneously) to PAN or ADR nephropathy completely inhibited p38 MAPK activation and attenuated ERK phosphorylation, with complete suppression of proteinuria. Electron microscopy and immunohistochemistry for nephrin and connexin43 revealed that podocyte injury was markedly ameliorated by FR167653. Furthermore, early treatment with FR167653 effectively prevented glomerulosclerosis and renal dysfunction in the chronic phase of ADR nephropathy. In cultured podocytes, PAN or oxidative stress induced the phosphorylation of p38 MAPK along with actin reorganization, and FR167653 inhibited such changes. These findings indicate that the activation of MAPK is necessary for podocyte injury, suggesting that p38 MAPK and, possibly, ERK should become a potential target for therapeutic intervention in proteinuric glomerulopathies.

J Am Soc Nephrol 16: 2690–2701, 2005. doi: 10.1681/ASN.2004121084

Podocytes are highly differentiated cells that form multiple interdigitating foot processes (1). They are interconnected by slit diaphragms and cover the glomerular basement membrane (GBM) surface. They stabilize glomerular architecture by counteracting the distension of the capillary wall and GBM (1) and maintain a large filtration surface through the slit diaphragms (2). Podocytes contribute to the specific size and charge filtration barrier, and their damage leads to the retraction of their foot processes and proteinuria (3,4).

Human acquired proteinuric glomerulopathies, such as minimal-change nephrotic syndrome (MCNS), focal segmental glomerulosclerosis (FSGS), and membranous nephropathy (MN), commonly exhibit foot process effacement of podocytes and loss of slit diaphragms in electron microscopy; these glomerulopathies therefore are considered as podocyte injury diseases (podocytopathies) (5). Several experimental models, such as rat puromycin aminonucleoside (PAN) nephropathy (6) and mouse adriamycin (ADR) nephropathy (7) that develop massive proteinuria resembling human minimal change disease, have provided insights into the cellular and intracellular mechanisms of podocyte injury disease. Recent advances coupled with molecular approaches have revealed crucial roles of slit diaphragm–associated proteins, including nephrin and podocin, in not only congenital but also acquired forms of proteinuric disorders (8,9). These studies have investigated the process or consequence of podocyte injury, but the mechanistic link between the pro-proteinuric insults and morphologic or functional impairment of podocytes remains to be fully understood.

The family of mitogen-activated protein kinases (MAPK), consisting of extracellular signal-regulated kinase (ERK), c-Jun N-terminal kinase (JNK), and p38, are activated by various extracellular stimuli, including growth factors and environmental stresses (10). The MAPK pathways involve multiple phosphorylation cascades, each of which mediates different signaling events either alone or in concert with other pathways (10). Especially, p38 MAPK is postulated to play a critical role

Received December 14, 2004. Accepted May 31, 2005.

Published online ahead of print. Publication date available at www.jasn.org.

Address correspondence to: Dr. Masashi Mukoyama, Department of Medicine and Clinical Science, Kyoto University Graduate School of Medicine, 54 Shogoin Kawahara-cho, Sakyo-ku, Kyoto 606-8507, Japan. Phone: +81-75-751-4285; Fax: +81-75-771-9452; E-mail: muko@kuhp.kyoto-u.ac.jp

ISSN: 1046-6673/1609-2690

in producing proinflammatory cytokines (11), mediating cell survival or apoptosis (12), and regulating the stability of cytoskeleton (13). These notions have prompted us to investigate the role of p38 MAPK in podocyte injury.

In this study, we investigated the alteration of p38 MAPK in disease states and reveal the activation of p38 MAPK at podocytes in clinical and experimental nephrotic syndromes, specifically from the preproteinuric state in the latter. Furthermore, we demonstrate that the treatment with FR167653, an inhibitor of p38 MAPK, in PAN nephropathy and ADR nephropathy completely abolishes proteinuria and prevents podocyte injury, suggesting that p38 MAPK activation is a common upstream mechanism necessary for podocyte injury in proteinuric glomerulopathies.

Materials and Methods

Antibodies

Primary antibodies used for Western blotting and immunohistochemical studies were rabbit anti–p38 MAPK, rabbit anti–phospho–p38 MAPK, rabbit anti-ERK, rabbit anti–phospho-ERK (Cell Signaling Technology, Boston, MA), rabbit anti-JNK, mouse anti–phospho-JNK (Santa Cruz Biotechnology, Santa Cruz, CA), mouse anti-nephrin (14), rabbit anti-nephrin (8), rabbit anti-connexin43 (Sigma, St. Louis, MO), mouse anti-synaptopodin (Progen, Heidelberg, Germany), and rabbit anti–TGF-β1 (Santa Cruz Biotechnology) antibodies.

Human Tissue Samples

Tissue samples were obtained at diagnostic renal biopsy performed at Kyoto University Hospital. We investigated the samples from patients who had MCNS, MN, and FSGS and were manifesting nephrotic-range proteinuria. As control human samples, we used nontumor tissues of the kidney from patients who had renal cell carcinoma and underwent nephrectomy or biopsy samples from the patients with minor glomerular abnormalities. The study was conducted under informed consent and was approved by the ethics committee on human research of Kyoto University Graduate School of Medicine.

Animal Experiments

All animal experiments were conducted in accordance with our institutional guidelines for animal research. For inducing rat PAN nephropathy, male Wistar-Kyoto rats that weighed 180 to 200 g received an intravenous injection of 50 mg/kg body wt PAN (Sigma) diluted in 0.9% saline. For inducing mouse ADR nephropathy, male BALB/c mice that weighed 20 to 25 g received an intravenous injection of 10 mg/kg body wt doxorubicin hydrochloride (Sigma) diluted in 0.9% saline. Control animals received vehicle only. Administration of FR167653 (Fujisawa Pharmaceutical, Osaka, Japan), a specific p38α MAPK inhibitor (15), was performed by subcutaneous injection (16) at a dose of 33 mg/kg body wt diluted in 0.5% methylcellulose (Sigma) daily from day −2 to day 14. In another series of experiments, daily FR167653 injection was started 10 min or 4 h after induction of the disease and continued for 2 wk (from day 0 to day 14) in these models. Control animals received an injection of methylcellulose alone.

Animals were fed a standard diet and given water *ad libitum*. We maintained these animals under alternating 12-h cycles of light and dark. Animals were killed on determined days after induction of the disease. Kidneys were harvested immediately for histologic and Western blot analyses.

Measurement of Blood and Urine Samples

Blood samples were obtained at the time of killing, and serum creatinine levels were measured using a kit (Wako, Osaka, Japan). For urine measurements, each animal was housed separately in a metabolic cage (Shinano Manufacturing, Tokyo, Japan) and daily urine volume was measured. Urinary albumin excretion was assayed with a rat or murine albumin ELISA kit (Exocell, Philadelphia, PA) (17).

Renal Histology and Electron Microscopy

Kidney sections were fixed with 4% buffered formaldehyde and embedded in paraffin as described (17,18). One-micrometer-thick sections were stained with periodic acid-Schiff and examined by light microscopy. Occurrence of the sclerotic glomeruli per section was assessed by counting the total number of glomeruli in a representative section from each sample. The procedure was performed by two investigators without knowledge of the origin of the slides, and the mean values were calculated.

For electron microscopy, small blocks of kidneys were fixed in 2.5% buffered glutaraldehyde, postfixed in 2% osmium tetroxide, dehydrated in graded ethanol, and embedded in epoxy resin (19). Ultrathin sections (0.1 μm thick) were stained with uranyl acetate and lead citrate and examined in an electron microscope (H-7600; Hitachi, Tokyo, Japan) at 75 kV.

Immunohistochemistry

For immunohistochemistry of phospho–p38 MAPK, kidney samples were fixed with 4% paraformaldehyde and embedded in paraffin. Three-micrometer sections were deparaffinized and rehydrated. Sections were treated with 0.3% H_2O_2 in methanol for 15 min to quench endogenous peroxide activity and were boiled at 100°C for 10 min in 10% citrate buffer to unmask antigens. Sections were incubated with anti–phospho–p38 MAPK at 4°C overnight and visualized using Vectastain ABC kit (Vector Laboratories, Burlingame, CA). Sections were counterstained with hematoxylin.

For immunofluorescence studies of nephrin and TGF-β1, 3-μm cryostat sections fixed with acetone were incubated for 1 h at 22°C with primary antibodies and stained with FITC-labeled anti-mouse or anti-rabbit IgG (Jackson Immunoresearch, West Grove, PA). For double staining of connexin43 and synaptopodin, sections were incubated with mixed primary antibodies and stained with FITC-labeled anti-rabbit IgG and TRITC-labeled anti-mouse IgG (Jackson Immunoresearch). Slides were examined with a confocal laser microscope (LSM5Pascal; Carl Zeiss, Munich, Germany) (19).

Western Blot Analysis

Glomeruli were isolated from the animals by graded sieving method (20). Western blot analysis was performed as described (17,18). In brief, isolated glomeruli or cells were lysed on ice in RIPA buffer that contained 10 μg/ml aprotinin, 2 mM dithiothreitol, 2 mM sodium orthovanadate, and 1 mM PMSF. Lysates were centrifuged at 15,000 rpm, and supernatants (50 μg protein/lane) were separated by 12.5% SDS-PAGE and transferred onto Immobilon filter (Millipore, Bedford, MA). After incubation with primary antibodies, immunoblots were developed with horseradish peroxidase–conjugated donkey anti-rabbit IgG (Amersham, Arlington Heights, IL) and a chemiluminescence kit (ECL plus; Amersham).

Cell Culture

A conditionally immortalized mouse podocyte cell line was provided by Dr. Peter Mundel (Albert Einstein College of Medicine, New York, NY) (21) and cultured as described (20). In brief, the cells were main-

tained at 33°C on dishes that were coated with collagen I (Koken, Tokyo, Japan), in RPMI 1640 medium (Nihonseiyaku, Tokyo, Japan) that contained 10% FBS (Sanko Junyaku, Tokyo, Japan) with 10 U/ml IFN-γ (Life Technologies BRL, Grand Island, NY). For differentiating podocytes, cells were cultured at 37°C with 5% FBS without IFN-γ for 2 wk. For experiment, cells were made quiescent in medium that contained 0.5% BSA (Sigma) for 24 h, pretreated with 10 μM FR167653 or vehicle 1 h before stimulation with 50 μg/ml PAN or 0.5 mM H_2O_2, and harvested at determined time after stimulation.

For analyzing actin cytoskeleton of cultured podocytes, cells were cultured on collagen I–coated coverslips in six-well dishes. For observation of F-actin filament, cells were fixed with 4% paraformaldehyde, incubated with 0.1% Triton X-100 for 10 min, and stained with 1 μM FITC-conjugated phalloidin (Sigma) for 30 min in darkness (21). Cover glasses were mounted, and the slides were examined by fluorescence microscopy.

Statistical Analyses

Data are expressed as means ± SEM. Statistical analysis was performed using ANOVA followed by Scheffe test. $P < 0.05$ was considered statistically significant.

Results

Enhanced Phosphorylation of p38 MAPK in Human and Rodent Podocyte Injury Diseases

In normal human kidneys, only a faint staining for phosphorylated p38 MAPK was observed in the glomeruli, mostly in the epithelial cells (Figure 1A). In proteinuric disorders, however, enhanced phosphorylation of p38 MAPK was detected at podocytes, as well as in parietal epithelial cells, as demonstrated in the biopsy specimens from the patients with MCNS (Figure 1B), MN (Figure 1C), and FSGS (Figure 1D). The mean occurrence of phospho–p38 MAPK–positive cells among nucleated cells per glomerulus (excluding parietal epithelial cells) was 5.2 ± 0.6, 11.1 ± 2.8, 18.2 ± 4.4, and 14.7 ± 4.8% in the samples from control kidney, MCNS, MN, and FSGS, respectively ($n = 3$ each).

We next examined rodent models of nephrotic syndrome. We found a marked increase of phosphorylated p38 MAPK in the isolated glomeruli of PAN nephropathy as well as ADR nephropathy on day 1 and day 3 (Figure 2, A and B), when urinary albumin excretion was still within normal range (see Figure 3, C and D). Enhanced phospho–p38 MAPK was confined mostly to podocytes (Figure 2, C and D). The mean occurrence of phospho–p38 MAPK–positive cells per glomerulus was 19.3 ± 1.9 and 16.7 ± 2.9% on day 1 in PAN and ADR nephropathy, respectively ($n = 4$ each). Thereafter, the levels of phospho–p38 MAPK got decreased and returned near the basal levels on day 7. We also examined the activation of other members of the MAPK family in these models of nephrotic syndrome. Phosphorylation of ERK (ERK-1 and -2) was increased in the glomeruli of PAN nephropathy on day 1 and day 3 and decreased on day 7, at a time course similar to that of p38 MAPK but with less pronounced activation (Figure 2E). Phosphorylation of JNK (JNK-1 and -2) was observed in the control glomeruli and unaltered during the course (Figure 2E). Essentially identical results for ERK and JNK changes were obtained in ADR nephropathy (data not shown). These findings indicate that p38 MAPK is markedly but transiently activated at podocytes before the appearance of overt proteinuria in rodent models of podocyte injury disease.

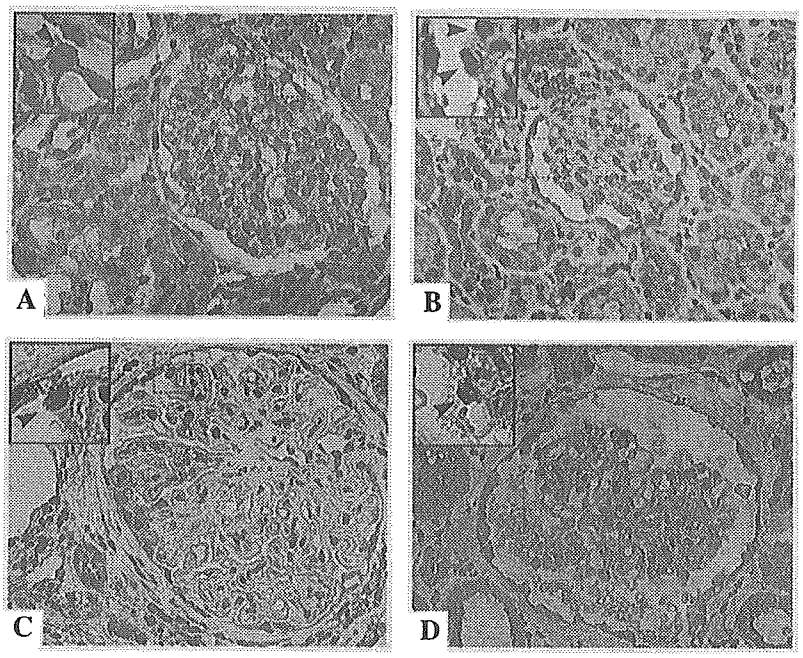

Figure 1. Phosphorylation of p38 mitogen-activated protein kinase (MAPK) in human glomerulopathies with podocyte injury. (A) In normal glomerulus, a weak staining for phospho–p38 MAPK was observed (arrowhead in inset). Enhanced phosphorylation of p38 MAPK was detected at nuclei of podocytes (arrowheads in insets) in the biopsy specimens from minimal-change disease (B), membranous nephropathy (C), and focal segmental glomerulosclerosis (D). Magnification, ×400; inset ×1000.

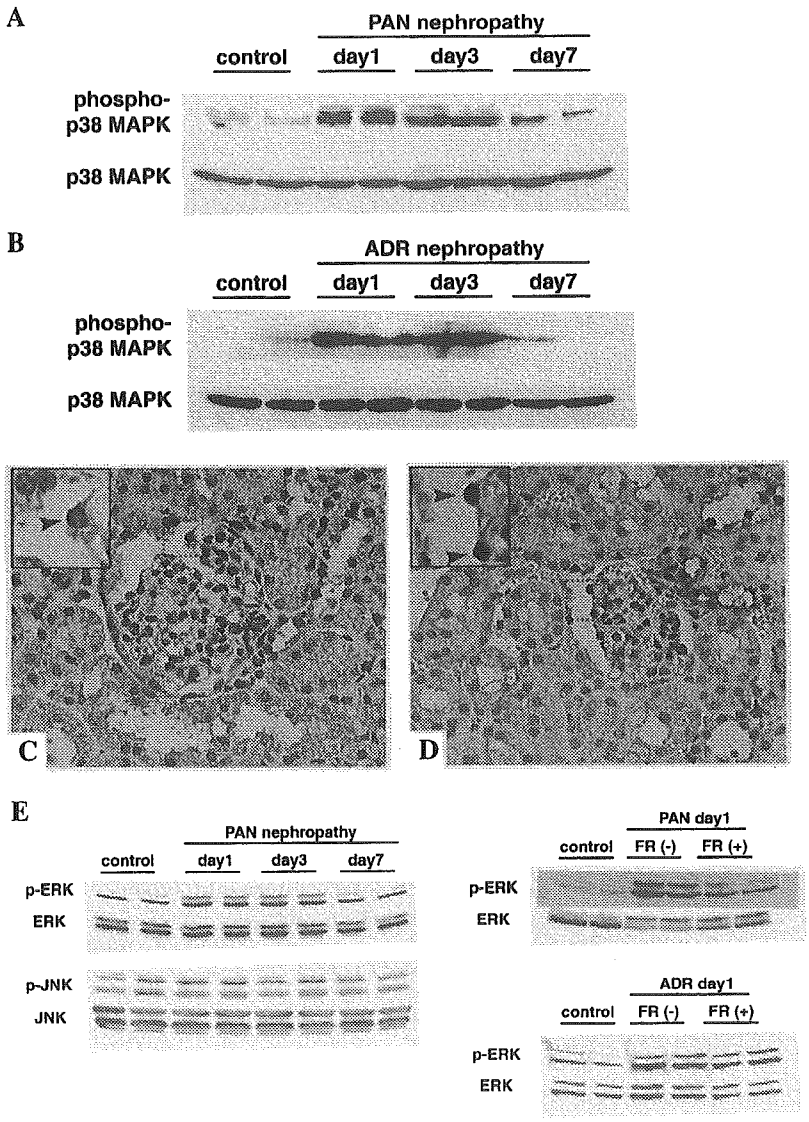

Figure 2. Phosphorylation of p38 MAPK in rat puromycin aminonucleoside (PAN) nephropathy and mouse adriamycin (ADR) nephropathy. Western blotting for phosphorylated p38 MAPK in glomeruli of rat PAN nephropathy (A) and mouse ADR nephropathy (B) revealed a marked increase on day 1 and day 3 and a significant decrease to almost basal levels on day 7. Blotting for total p38 MAPK was performed as internal control. Immunohistochemistry for phospho–p38 MAPK on day 1 of PAN nephropathy (C) and ADR nephropathy (D) revealed that enhanced phospho–p38 MAPK was confined mostly to podocytes (arrowheads). (E, Left) Western blotting for phosphorylated p44 and p42 extracellular signal-regulated kinase (ERK; ERK-1 and -2) and phosphorylated p46 and p54 c-Jun N-terminal kinase (JNK; JNK-1 and -2) in glomeruli of rat PAN nephropathy. (Right) Effects of FR167653 administration on phospho-ERK levels in glomeruli of PAN nephropathy and ADR nephropathy on day 1. Magnification, ×400 in C and D; ×1000 in C and D inset.

Urinary Albumin Excretion in PAN and ADR Nephropathy

In rats with PAN nephropathy, no overt proteinuria was observed until day 4. Urinary albumin excretion showed a significant increase on day 7, peaked at approximately day 14, and returned to almost normal range by day 28 (Figure 3C). In mice with ADR nephropathy, urinary albumin excretion was normal until day 4, was significantly increased on day 7, reached to the peak level at approximately day 14, and remained significantly elevated through day 28 (Figure 3D). Such time courses were compatible with those in previous reports (6,7).

Effect of p38 MAPK Inhibitor on Proteinuria in PAN and ADR Nephropathy

Because the phosphorylation of p38 MAPK at podocytes preceded the onset of overt proteinuria, we hypothesized that the activation of p38 MAPK would critically be relevant to the appearance of proteinuria in these models of podocyte injury disease. We therefore investigated the effect of administration of FR167653, a specific inhibitor of p38 MAPK (15,16), to PAN and ADR nephropathy models on their renal outcomes. FR167653 has been reported to selectively inhibit p38α MAPK activity *in vitro*, without affecting the activities of other kinases,

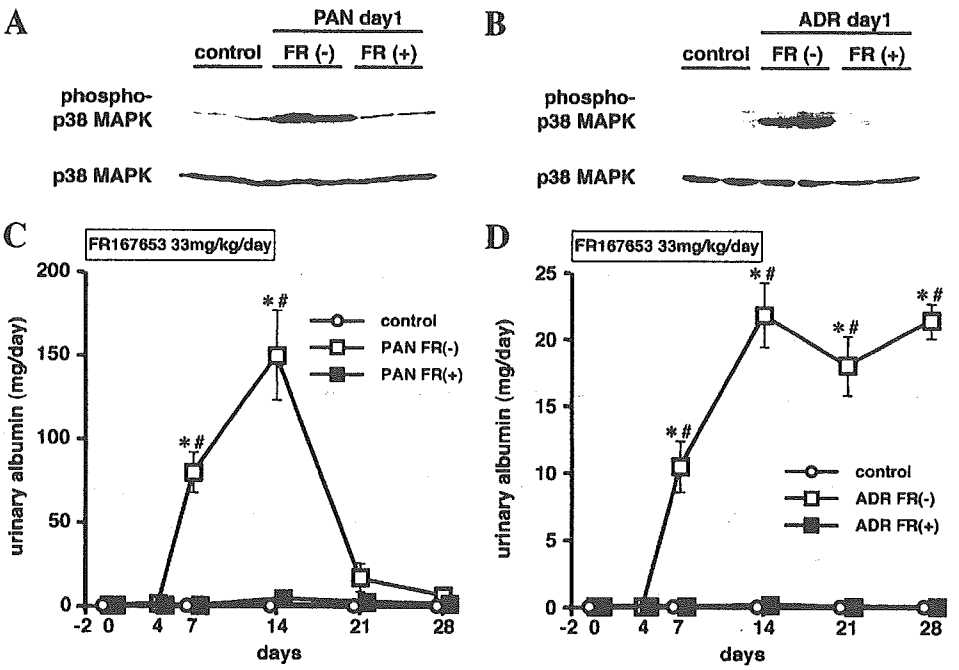

Figure 3. Effects of FR167653 administration on phospho–p38 MAPK levels in glomeruli and proteinuria in PAN nephropathy and ADR nephropathy. (A and B) Administration of FR167653 to animals with PAN nephropathy or ADR nephropathy abolished enhanced phosphorylation of p38 MAPK on day 1. (C and D) Urinary albumin excretion in nephrotic animals with or without FR167653. (C) In PAN nephropathy, urinary albumin increased on day 7, peaked at approximately day 14, and then decreased (□). Daily subcutaneous injection (day −2 to day 14) of FR167653 to rats with PAN nephropathy almost completely suppressed albumin excretion (■) to the control level (○). Mean ± SEM. $^*P < 0.05$ *versus* control; $^\#P < 0.05$ *versus* FR167653 treatment; $n = 7$. (D) In ADR nephropathy, urinary albumin increased on day 7, peaked at approximately day 14, and remained high through day 28 (□). Administration of FR167653 to mice with ADR nephropathy completely suppressed albumin excretion (■) to the control level (○). Mean ± SEM. $^*P < 0.05$ *versus* control; $^\#P < 0.05$ *versus* FR167653 treatment; $n = 7$.

including p38γ; ERK-1; JNK-2; protein kinases A, C, and G; and epidermal growth factor receptor (EGFR) kinase, as well as exerting no inhibitory effect on cyclooxygenase-1 or -2 activities, even at a dose 2 orders of magnitude higher than that for p38α MAPK inhibition (15).

In the glomeruli isolated from the animals that were pretreated with FR167653 from day −2, enhanced phosphorylation of p38 MAPK was effectively abolished to the control levels (Figure 3, A and B), indicating that the dose administered was sufficient to inhibit the activation of p38 MAPK at glomeruli *in vivo*. In this condition, we observed substantial inhibitory effects on the enhanced phosphorylation of ERK by administration of FR167653 in both models (Figure 2E, right), but the effects were less pronounced as compared with the effect on p38 MAPK; FR167653 did not affect JNK phosphorylation (data not shown). By daily subcutaneous administration of this compound to rats with PAN nephropathy for 17 d, urinary albumin excretion was almost completely suppressed to the control level (Figure 3C). Furthermore, in mice with ADR nephropathy, the administration of FR167653 for the same period completely abrogated the increase of urinary albumin excretion as well (Figure 3D). Thus, the blockade of p38 MAPK activation with FR167653 potently inhibited proteinuria in both models of podocyte injury disease, irrespective of initiating insults.

We next examined the effect of FR167653 administration after induction of the disease. When the compound was administered 4 h after induction of the diseases, FR167653 failed to suppress significantly the enhanced phosphorylation of p38 MAPK observed on day 1 (data not shown) in both models or subsequent increase in urinary albumin excretion (PAN day 14: 149.4 ± 26.8 *versus* 129.4 ± 18.8 mg/d; ADR day 14: 21.8 ± 2.6 *versus* 14.3 ± 2.1 mg/d; ADR day 28: 21.4 ± 1.5 *versus* 15.9 ± 3.8 mg/d; vehicle *versus* FR167653 treatment, respectively, $n = 4$). When the compound was injected 10 min after the induction of ADR nephropathy, half of the animals exhibited significant inhibition of phospho–p38 MAPK activation and effective suppression of the proteinuria near the control levels, but the rest showed almost no effect on p38 MAPK phosphorylation or proteinuria ($n = 3$ each).

Effect of p38 MAPK Inhibitor on Podocyte Injury

We next investigated the morphologic changes with or without inhibition of p38 MAPK. In electron microscopic analysis, the glomeruli with PAN nephropathy 2 wk after onset showed foot process effacement, with occasional vacuolation of podocytes (Figure 4A, middle). By contrast, glomeruli from FR167653-treated rats with PAN nephropathy revealed that foot processes were almost intact as in the control (Figure 4A). Likewise, glomeruli from mice with ADR nephropathy showed

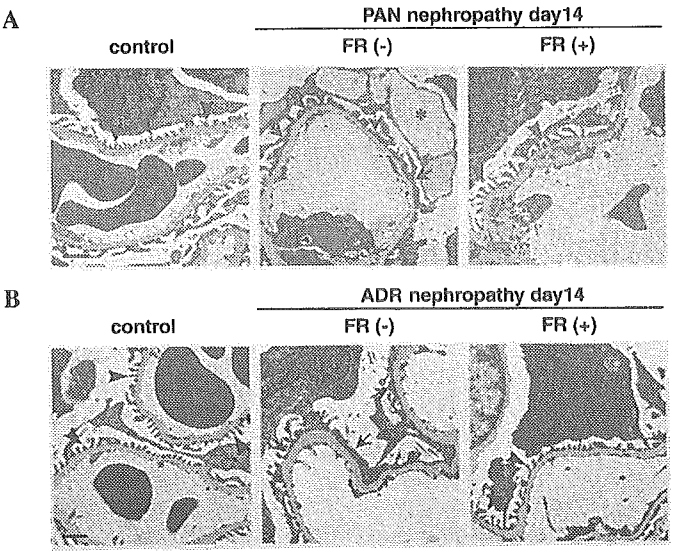

Figure 4. Electron microscopy of the glomerulus in podocyte injury models with or without FR167653. (A) Podocytes in control rats showed intact foot processes (arrowheads). PAN-treated rats on day 14 revealed foot process effacement (arrows), with occasional vacuolation of podocytes (*). In FR167653-administered rats with PAN nephropathy, most of the foot processes were intact [FR(+); arrowheads]. (B) Podocytes in control mice showed intact foot processes (arrowheads). Mice with ADR nephropathy on day 14 also showed foot process effacement (arrows), whereas FR167653 treatment retained normal foot processes [FR(+), arrowheads]. Bar = 1 μm.

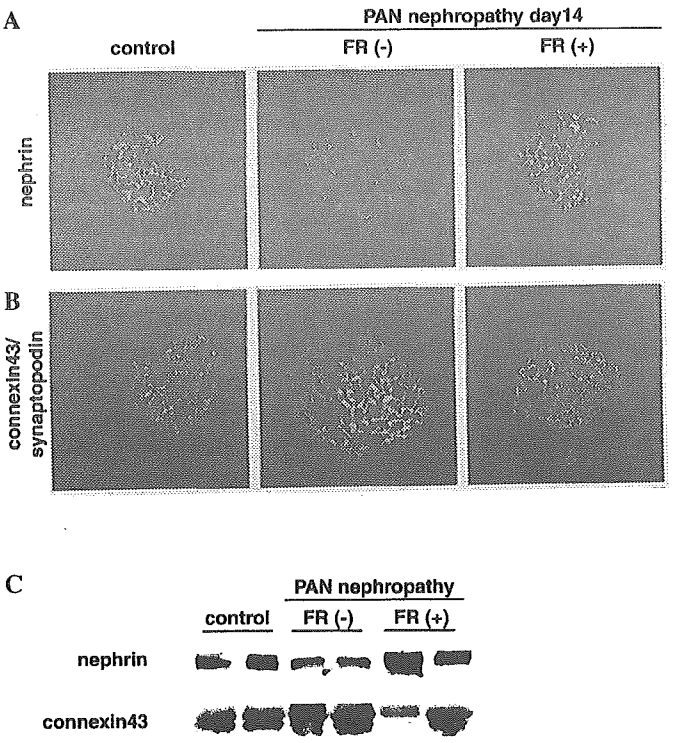

Figure 5. Expression of nephrin and connexin43 in PAN nephropathy with or without FR167653 on day 14. (A) Immunofluorescence study for nephrin. Normal glomerulus showed a linear staining pattern for nephrin along the capillary wall. PAN nephropathy revealed decreased intensity with a coarse granular pattern for nephrin. FR167653 treatment retained a normal linear pattern. (B) Immunofluorescence study for connexin43 (green) merged with synaptopodin (red). Podocytes in the control glomerulus rarely expressed connexin43. PAN nephropathy showed increased expression of connexin43 at podocytes. FR167653 treatment reduced its expression. (C) Western blotting for nephrin and connexin43 in glomeruli of PAN nephropathy with or without FR167653. Nephrin was decreased in PAN nephropathy, whereas FR167653 treatment showed no reduction in nephrin expression. By contrast, connexin43 was increased in PAN nephropathy, whereas FR167653 treatment decreased connexin43 expression to the control level.

marked foot process effacement, and the treatment with FR167653 prevented such changes (Figure 4B).

Nephrin, a product of the gene mutated in congenital nephrotic syndrome (22), is decreased and its distribution is altered upon proteinuric conditions in human nephrotic syndrome (23) and in animal models (8). We therefore investigated the expression and distribution pattern of nephrin in experimental animals. In Western blot and immunofluorescence analyses, rats with PAN nephropathy exhibited the decreased expression of nephrin on day 14, although FR167653-treated animals showed no reduction in nephrin expression (Figure 5, A and C). By immunofluorescence study, normal glomeruli showed a linear staining pattern for nephrin along the capillary wall, whereas glomeruli with PAN nephropathy exhibited a coarse granular staining pattern (Figure 5A). Rats that had PAN nephropathy and were treated with FR167653, however, retained such a linear pattern as seen in normal glomeruli (Figure 5A).

Connexin43 is a major gap junction protein that is expressed most abundantly among the connexin family in the kidney (24). Its expression is upregulated at podocytes upon injury (24) and therefore postulated as a marker for podocyte injury (19,24). We observed increased connexin43 in glomeruli with PAN nephropathy by Western blot and immunofluorescence analyses (Figure 5, B and C). By double-labeling immunofluorescence, glomerular expression of connexin43 in rats with PAN nephropathy merged with synaptopodin, a podocyte marker (21) (Figure 5B). FR167653 treatment in rats with PAN nephropathy reduced connexin43 expression at podocytes near the control level (Figure 5, B and C). Taken together, the administration of FR167653 in these rodent models of nephrotic syndrome prevented podocyte injury.

Effect of p38 MAPK Inhibitor on Glomerulosclerosis in ADR Nephropathy

By long-term follow-up of ADR nephropathy up to day 56, we observed persistent proteinuria (urinary albumin, 5.13 ± 1.49 mg/d; Figure 6A), together with chronic histologic changes such as tubular atrophy and focal glomerulosclerosis (Figure 6, B and C). The occurrence of sclerotic glomeruli out of total glomeruli per section showed a markedly higher rate in ADR nephropathy (Figure 6E). Some nonsclerotic glomeruli of

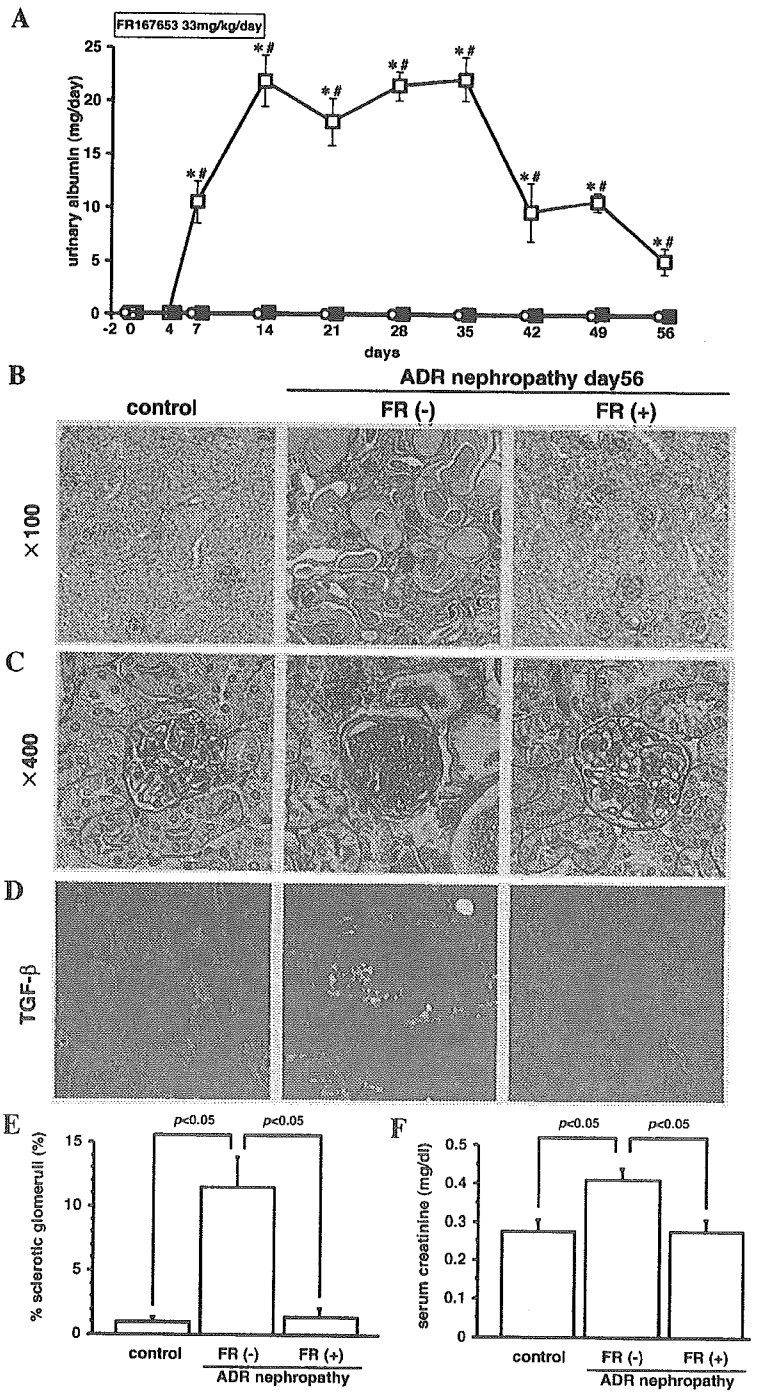

Figure 6. Effects of FR167653 administration on renal histology and function in mice with ADR nephropathy. (A) In ADR nephropathy, urinary albumin excretion persisted until day 56 (□). FR167653 treatment in these mice prevented overt albuminuria throughout the course (■), whose levels were similar to the control (○). Mean ± SEM. $^{*}P < 0.05$ *versus* control; $^{\#}P < 0.05$ *versus* FR167653 treatment; $n = 4$ to 7. (B) ADR nephropathy showed massive protein casts with marked tubular atrophy and degeneration. Administration of FR167653 revealed almost normal feature. (C) ADR nephropathy showed focal glomerulosclerosis, whereas FR167653 treatment revealed few sclerotic glomeruli. (D) Immunofluorescence study for TGF-β1. Some nonsclerotic glomeruli of ADR nephropathy exhibited an enhanced expression of TGF-β1, probably in the mesangial area. No glomeruli of FR167653-treated mice expressed TGF-β1. (E) The occurrence of sclerotic glomeruli on day 56 out of total glomeruli per section showed a markedly higher rate in ADR nephropathy than in control and FR167653 treatment. Mean ± SEM; $n = 4$. (F) The serum creatinine level on day 56 was significantly elevated in ADR nephropathy, but it remained normal with FR167653 treatment. Mean ± SEM; $n = 4$. Magnification, ×100 in B; ×400 in C, periodic acid-Schiff stain on day 56.

ADR nephropathy exhibited an enhanced glomerular expression of TGF-β1 (Figure 6D). Serum creatinine levels were also significantly elevated in ADR nephropathy (Figure 6F). Administration of FR167653 to mice with ADR nephropathy during the first 2 wk, however, maintained normal albumin excretion throughout the observation period (urinary albumin, 0.12 ± 0.07 mg/d on day 56; Figure 6A). Moreover, the treatment resulted in almost normal renal histology (Figure 6, B, C, and E), no glomerular augmentation of TGF-β1 (Figure 6D), and normal renal function (Figure 6F). Thus, FR167653 prevented the development of glomerulosclerosis and chronic renal dysfunction.

Effect of p38 MAPK Inhibitor on Actin Reorganization in Cultured Mouse Podocytes

Next we examined the effect of p38 MAPK activation on morphologic changes of podocytes using cultured mouse podocytes. Treatment of podocytes with PAN caused the phosphorylation of p38 MAPK (Figure 7A, left) and facilitated actin reorganization (Figure 7B). Pretreatment with FR167653 abolished the phosphorylation of p38 MAPK (Figure 7A) and prevented actin reorganization (Figure 7B). Likewise, the stimulation of podocytes with H_2O_2 as oxidative stress that activates p38 MAPK (10) increased phospho–p38 MAPK (Figure 7A, right) together with actin reorganization (Figure 7C). Pretreatment with FR167653 prevented these changes as well (Figure 7, A and C). Thus, the blockade of p38 MAPK activation inhibited actin reorganization.

Discussion

In this study, we investigated the significance of p38 MAPK in podocyte injury in clinical as well as experimental nephropathies and revealed that p38 MAPK activation at podocytes plays a crucial role for its pathophysiology. We showed an enhanced phosphorylation of p38 MAPK in glomeruli of clinical nephrotic syndrome. Furthermore, we demonstrated an essential role of p38 MAPK activation in rodent models of podocyte injury disease. In PAN nephropathy and ADR nephropathy, enhanced phosphorylation of p38 MAPK in the glomeruli was found during the first week of insult preceding overt proteinuria, and inhibition of p38 MAPK by FR167653

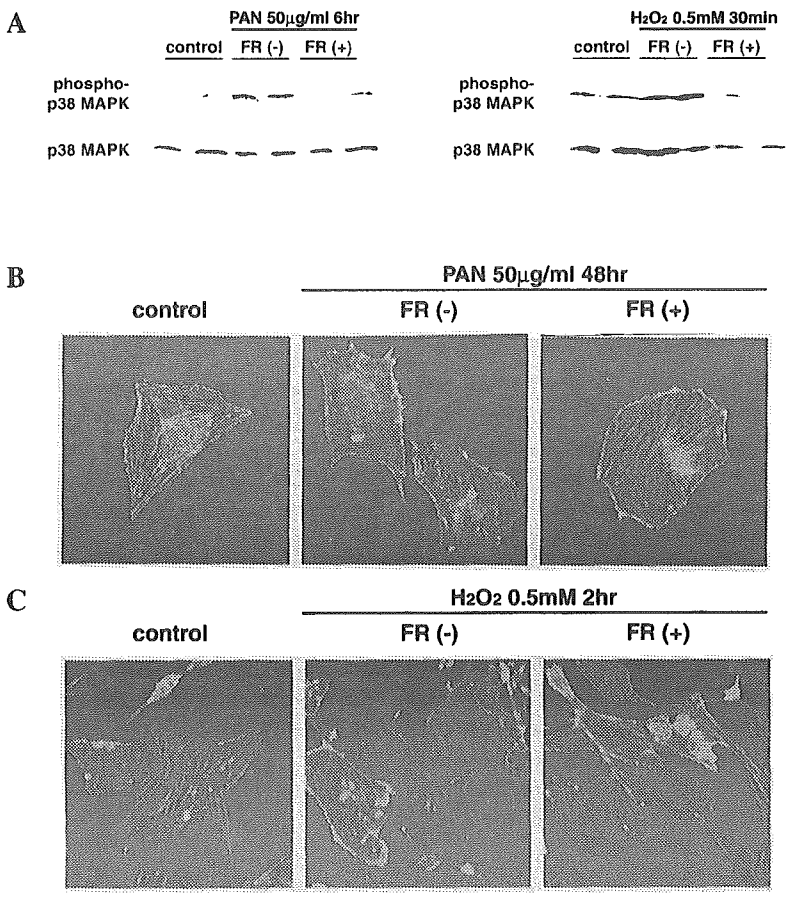

Figure 7. Effects of FR167653 on actin reorganization induced by PAN or oxidative stress. (A) In cultured podocytes, stimulation with PAN (50 μg/ml) for 6 h caused the phosphorylation of p38 MAPK. Pretreatment with FR167653 (10 μM) abolished p38 MAPK phosphorylation (left). Stimulation with H_2O_2 (0.5 mM) also increased phospho–p38 MAPK at 30 min, and pretreatment with FR167653 abrogated such increase (right). (B) Stimulation with PAN for 48 h caused actin reorganization in cultured podocytes, and pretreatment with FR167653 prevented actin reorganization. (C) Stimulation with H_2O_2 for 2 h also caused actin reorganization, which was prevented by FR167653 pretreatment.

resulted in marked suppression of podocyte injury and proteinuria. Moreover, the treatment with FR167653 during an early phase effectively prevented the progression of renal histologic changes in the chronic phase of ADR nephropathy. These findings strongly suggest that p38 MAPK activation should be functionally relevant to the pathogenesis of podocyte injury, serving as an upstream event necessary for proteinuria.

We observed an enhanced phosphorylation of p38 MAPK in human nephrotic states mainly in podocytes (Figure 1). It has already been reported that p38 MAPK activation in podocytes and tubules is found in various human nonproliferative as well as proliferative glomerulonephritis and correlates well with the degree of proteinuria and glomerular and/or interstitial injury (25). We also observed an enhanced p38 MAPK phosphorylation in podocytes of rodent models of nephrotic syndrome, especially during an early phase of the disease (Figure 2). It should be noted that there seems to be discrepancy between clinical nephropathies with sustained p38 MAPK phosphorylation and these rodent models with only transient activation of p38 MAPK. One explanation could be the difference in the cause and time course of podocyte injury. In experimental nephropathies, activation of p38 MAPK is elicited by a single burst of noxious stimulus, *i.e.*, injection of PAN or ADR, but in human glomerulopathies, p38 MAPK activation may be prolonged because of continuous stimuli such as circulating immune complexes. Although circumstantial, this might be reflected in different time courses of proteinuria between these models and clinical conditions. However, the pathogenic role for prolonged p38 MAPK activation in causing proteinuria and podocyte injury seen in clinical nephrotic syndrome should await further clarification.

In our study, there might be the time dissociation between p38 MAPK phosphorylation that occurred very early in these models and the appearance of overt proteinuria that occurred several days later (Figures 2 and 3). It is well conceivable that the activation of p38 MAPK in podocytes should trigger several intracellular signaling cascades, giving rise to serial reactions of the genes and proteins that alter cytoskeleton integrity or barrier function and finally lead to overt proteinuria. Proteinuria may ensue well behind (*e.g.*, months later) the transient activation and subsidence of triggering events, as shown in the ischemia/reperfusion injury model (26). In addition, a causal relationship between the only brief activation of p38 MAPK and the morphologic changes occurring several days later has been demonstrated in other cell types (27,28). Although the pretreatment by FR167653 in this study abrogated both the p38 MAPK activation and proteinuria, delayed FR167653 administration resulted in much less effect on proteinuria in parallel with the less efficient p38 MAPK inhibition (approximately 50% inhibition on both parameters when administered just after induction). These data may also suggest a close association between p38 MAPK activation and proteinuria.

Specificity of the inhibitor FR167653 for p38 MAPK is another issue to be addressed. Because this compound has been shown to selectively inhibit p38α MAPK without affecting ERK-1, JNK-2, or cyclooxygenase-1 and -2 *in vitro* (15), it is reasonable to assume that the results obtained here would be due to the specific inhibition of p38 MAPK (Figure 3A). The *in vivo* specificity of this compound, however, is not fully characterized. It is interesting that we found that FR167653 treatment attenuated ERK phosphorylation substantially, although not completely (Figure 2E), along with the complete inhibition of p38 MAPK activation. It is not clear at present whether such attenuation was direct and somehow contributed to the beneficial effects of this compound. Alternatively, ERK may have been downregulated secondary to p38 MAPK inhibition, as shown in thrombin-stimulated ERK activation in endothelium (29). Nevertheless, we cannot exclude the possibility that the beneficial effects of FR167653 exerted in this study could be due to either p38 MAPK or ERK pathway inhibition or both.

Activation of p38 MAPK is observed in embryonic kidneys and is required for renal development in rats (30). Although MAPK are thought to be largely inactive in adult kidneys at normal conditions, the activation of p38 MAPK can be detected in diseased kidneys from experimental models (16,31,32) and various human nephropathies (25,32,33). The role of p38 MAPK activation has been investigated so far by pharmacologic blockade in several experimental models. For example, p38 MAPK inhibition reduced proteinuria in anti-GBM glomerulonephritis (16) and ameliorated renal ischemia/reperfusion injury (34). In addition, blockade of p38 MAPK diminished angiotensin II–mediated renal damage, reducing mesangial matrix expansion (35). These reports have suggested that p38 MAPK should play important roles in cell proliferation or inflammatory responses in the mesangium and tubulointerstitium. In one report using complement-mediated cell injury, inhibition of p38 MAPK 7 d after induction of the disease failed to reverse and rather augmented cytotoxicity, suggesting that the activated p38 MAPK in podocytes may be cytoprotective during a later phase of this model (36). These studies, however, have not addressed the involvement of p38 MAPK in the pathogenesis of podocytopathies. In our study, we first demonstrate the pathogenic role of p38 MAPK activation in podocyte injury and proteinuria *in vivo* and effective prevention of the disease by an early inhibition of this activation. Furthermore, we reveal that the reduced expression of nephrin was effectively reversed by the treatment (Figure 5). Because nephrin expression largely correlates inversely with the degree of proteinuria (8,23), this perhaps may be an indirect consequence of inhibited proteinuria. Further study is needed to explore the relationship between nephrin expression and p38 MAPK activation.

In podocytes, several reports already investigated the role of p38 MAPK using conditionally immortalized mouse podocyte culture. p38 MAPK mediated TGF-β–induced apoptosis in podocytes (37). Because podocyte loss is a key event leading to glomerulosclerosis (38), p38 MAPK activation may facilitate glomerulosclerosis. High glucose exposure to podocytes stimulated p38 MAPK phosphorylation and α5(IV) collagen expression *via* the 12-lipoxygenase–dependent pathway (39). Furthermore, mechanical stretch induced the upregulation of cyclooxygenase-2 and prostaglandin EP4 receptor in a p38 MAPK–dependent manner (40), which may facilitate actin depolymerization (40). In addition, high glucose to podocytes stimulates the expression of vascular endothelial growth factor

(41), which in turn induces α3(IV) collagen production, acting downstream of TGF-β1 (42). Of note, in mesangial cells, vascular endothelial growth factor is induced by TGF-β1 *via* the p38 MAPK–dependent pathway and stimulates collagen and fibronectin expression (43). Whether such pathways are critically involved in the current beneficial effects exerted by p38 MAPK inhibition *in vivo* is not clear and requires further investigation.

How does p38 MAPK activation affect actin cytoskeleton and induce podocyte injury? By using cultured podocytes, we demonstrated a close association between p38 MAPK activation and actin reorganization induced by PAN or oxidative stress *in vitro*, and such changes were effectively abrogated by p38 MAPK inhibition (Figure 7). Therefore, one of the possibilities is that p38 MAPK activation may depolymerize actin filament through the molecule(s) that modulates actin polymerization. Several specific substrates for p38 MAPK that may be physiologically relevant have been identified. These include transcriptional factors ATF-2, CHOP, Elk-1, MEF2A, MEF2C, and Max, which can be phosphorylated and activated by p38 MAPK (10,44). p38 MAPK can also activate MAPK–activated protein kinases 2 and 3, which in turn phosphorylate small heat-shock protein 27 (hsp27) (10,13). Hsp27 is importantly involved in actin filament dynamics regulated by p38 MAPK (13), and the phosphorylated level of hsp27 is critically relevant to the morphologic changes and actin depolymerization in podocytes (45). Actin filament is a major constituent of foot processes, and depolymerization of actin filaments leads to foot process effacement (46). Because actin filaments interact with components of slit diaphragm and with integrins (46), depolymerized actin filaments may facilitate the loss of adhesive interactions, leading to disruption of slit diaphragm and detachment from GBM. Although p38 MAPK activation can induce actin reorganization *in vitro*, their molecular link is not demonstrated *in vivo*, and which molecular mechanisms are in fact involved in our study is unclear. Because the cell line of cultured podocytes used in this study does not form interdigitated foot processes or slit diaphragm (45), it will be required to establish the culture system reproducing the *in vivo* podocyte phenotypes to answer these questions.

Podocyte dysfunction leads to progressive renal insufficiency. First, podocyte damage causes proteinuria. Sustained proteinuria gives rise to tubulointerstitial injury, eventually leading to renal failure (47). Second, podocyte injury impairs mesangial structure and function. In anti–Thy-1 glomerulonephritis, a reversible self-limiting model in itself, preceding minor podocyte injury with PAN pretreatment results in irreversible mesangial alteration (48). We showed recently that cysteine-rich protein 61 (Cyr61), a potent angiogenic protein that belongs to the CCN family of matrix-associated secreted protein family, is expressed in podocytes and upregulated in anti–Thy-1 glomerulonephritis (20). Cyr61 inhibits mesangial cell migration, suggesting that Cyr61 may play a modulatory role in limiting mesangial activation (20). Thus, podocytes may secrete various humoral factors that regulate mesangial structure and function, and their reduction could result in impaired mesangial function such as mesangial proliferation and matrix expansion. Third, podocyte loss or detachment from the GBM leads to glomerulosclerosis (38). In human diabetic nephropathy and IgA nephropathy, decreased podocyte number correlates significantly with poor prognosis (49,50). These studies suggest that podocyte injury is critical not only in podocyte-specific diseases such as MCNS and FSGS but also in podocyte-nonspecific diseases such as IgA nephropathy.

In conclusion, our study reveals that the activation of p38 MAPK is crucial for podocyte injury in experimental nephrotic syndrome, suggesting that p38 MAPK activation is a common upstream mechanism necessary for podocyte injury in various proteinuric glomerulopathies. Although we need to be cautious in interpreting these results and extrapolating them to clinical situations, our study opens up a possibility that p38 MAPK and, possibly, ERK could become potential targets for therapeutic intervention in proteinuric glomerulopathies.

Acknowledgments

This work was supported in part by research grants from the Japanese Ministry of Education, Culture, Sports, Science and Technology; the Japanese Ministry of Health, Labor and Welfare; Smoking Research Foundation; and the Salt Science Research Foundation.

We gratefully acknowledge Dr. Peter Mundel (Albert Einstein College of Medicine, Bronx, NY) for the immortalized podocyte cell line, Dr. Sumio Kiyoto (Fujisawa Pharmaceutical, Osaka, Japan) for providing FR167653, and Drs. Shunji Nakatsuji and Yuji Oishi (Fujisawa Pharmaceutical) for electron microscopic analysis. We are also grateful to Junko Nakamura and Saori Saito for technical assistance and Shigeka Doi, Atsuko Sonoda, and Junichi Nomura for secretarial assistance.

References

1. Kriz W, Hackenthal E, Nobiling R, Sakai T, Elger M: A role for podocytes to counteract capillary wall distension. *Kidney Int* 45: 369–376, 1994
2. Drumond MC, Kristal B, Myers BD, Deen WM: Structural basis for reduced glomerular filtration capacity in nephrotic humans. *J Clin Invest* 94: 1187–1195, 1994
3. Laurens W, Battaglia C, Foglieni C, De Vos R, Malanchini B, Van Damme B, Vanrenterghem Y, Remuzzi G, Remuzzi A: Direct podocyte damage in the single nephron leads to albuminuria in vivo. *Kidney Int* 47: 1078–1086, 1995
4. Pavenstadt H: The charge for going by foot: Modifying the surface of podocytes. *Exp Nephrol* 6: 98–103, 1998
5. Barisoni L, Mundel P: Podocyte biology and the emerging understanding of podocyte diseases. *Am J Nephrol* 23: 353–360, 2003
6. Ryan GB, Karnovsky MJ: An ultrastructural study of the mechanisms of proteinuria in aminonucleoside nephrosis. *Kidney Int* 8: 219–232, 1975
7. Wang Y, Wang YP, Tay YC, Harris DC: Progressive adriamycin nephropathy in mice: Sequence of histologic and immunohistochemical events. *Kidney Int* 58: 1797–1804, 2000
8. Kawachi H, Koike H, Kurihara H, Yaoita E, Orikasa M, Shia MA, Sakai T, Yamamoto T, Salant DJ, Shimizu F: Cloning of rat nephrin: Expression in developing glomeruli and in proteinuric states. *Kidney Int* 57: 1949–1961, 2000
9. Kawachi H, Koike H, Kurihara H, Sakai T, Shimizu F: Cloning of rat homologue of podocin: Expression in pro-

teinuric states and in developing glomeruli. *J Am Soc Nephrol* 14: 46–56, 2003
10. Widmann C, Gibson S, Jarpe MB, Johnson GL: Mitogen-activated protein kinase: Conservation of a three-kinase module from yeast to human. *Physiol Rev* 79: 143–180, 1999
11. Adams JL, Badger AM, Kumar S, Lee JC: p38 MAP kinase: Molecular target for the inhibition of pro-inflammatory cytokines. *Prog Med Chem* 38: 1–60, 2001
12. Kimura C, Zhao QL, Kondo T, Amatsu M, Fujiwara Y: Mechanism of UV-induced apoptosis in human leukemia cells: Roles of Ca2+/Mg2+-dependent endonuclease, caspase-3, and stress-activated protein kinases. *Exp Cell Res* 239: 411–422, 1998
13. Guay J, Lambert H, Gingras-Breton G, Lavoie JN, Huot J, Landry J: Regulation of actin filament dynamics by p38 MAP kinase-mediated phosphorylation of heat shock protein 27. *J Cell Sci* 110: 357–368, 1997
14. Orikasa M, Matsui T, Oite T, Shimizu F: Massive proteinuria induced in rats by a single intravenous injection of a monoclonal antibody. *J Immunol* 141: 807–814, 1998
15. Takahashi S, Keto Y, Fujita T, Uchiyama T, Yamamoto A: FR167653, a p38 mitogen-activated protein kinase inhibitor, prevents *Helicobacter pylori*-induced gastritis in Mongolian gerbils. *J Pharmacol Exp Ther* 296: 48–56, 2001
16. Wada T, Furuichi K, Sakai N, Hisada Y, Kobayashi K, Mukaida N, Tomosugi N, Matsushima K, Yokoyama H: Involvement of p38 mitogen-activated protein kinase followed by chemokine expression in crescentic glomerulonephritis. *Am J Kidney Dis* 38: 1169–1177, 2001
17. Suganami T, Mukoyama M, Sugawara A, Mori K, Nagae T, Kasahara M, Yahata K, Makino H, Fujinaga Y, Ogawa Y, Tanaka I, Nakao K: Overexpression of brain natriuretic peptide in mice ameliorates immune-mediated renal injury. *J Am Soc Nephrol* 12: 2652–2663, 2001
18. Yokoi H, Mukoyama M, Nagae T, Mori K, Suganami T, Sawai K, Yoshioka T, Koshikawa M, Nishida T, Takigawa M, Sugawara A, Nakao K: Reduction in connective tissue growth factor by antisense treatment ameliorates renal tubulointerstitial fibrosis. *J Am Soc Nephrol* 15: 1140–1150, 2004
19. Suganami T, Mukoyama M, Mori K, Yokoi H, Koshikawa M, Sawai K, Hidaka S, Ebihara K, Tanaka T, Sugawara A, Kawachi H, Vinson C, Ogawa Y, Nakao K: Prevention and reversal of renal injury by leptin in a new mouse model of diabetic nephropathy. *FASEB J* 19: 127–129, 2005
20. Sawai K, Mori K, Mukoyama M, Sugawara A, Suganami T, Koshikawa M, Yahata K, Makino H, Nagae T, Fujinaga Y, Yokoi H, Yoshioka T, Yoshimoto A, Tanaka I, Nakao K: Angiogenic protein Cyr61 is expressed by podocytes in anti-Thy-1 glomerulonephritis. *J Am Soc Nephrol* 14: 1154–1163, 2003
21. Mundel P, Reiser J, Zuniga Mejia Borja A, Pavenstadt H, Davidson GR, Kriz W, Zeller R: Rearrangements of the cytoskeleton and cell contacts induce process formation during differentiation of conditionally immortalized mouse podocyte cell lines. *Exp Cell Res* 236: 248–258, 1997
22. Kestila M, Lenkkeri U, Mannikko M, Lamerdin J, McCready P, Putaala H, Ruotsalainen V, Morita T, Nissinen M, Herva R, Kashtan CE, Peltonen L, Holmberg C, Olsen A, Tryggvason K: Positionally cloned gene for a novel glomerular protein—nephrin—is mutated in congenital nephrotic syndrome. *Mol Cell* 1: 575–582, 1998
23. Furness PN, Hall LL, Shaw JA, Pringle JH: Glomerular expression of nephrin is decreased in acquired human nephrotic syndrome. *Nephrol Dial Transplant* 14: 1234–1237, 1999
24. Yaoita E, Yao J, Yoshida Y, Morioka T, Nameta M, Takata T, Kamiie J, Fujinaka H, Oite T, Yamamoto T: Up-regulation of connexin43 in glomerular podocytes in response to injury. *Am J Pathol* 161: 1597–1606, 2002
25. Stambe C, Nikolic-Paterson DJ, Hill PA, Dowling J, Atkins RC: p38 Mitogen-activated protein kinase activation and cell localization in human glomerulonephritis: Correlation with renal injury. *J Am Soc Nephrol* 15: 326–336, 2004
26. Takada M, Chandranker A, Nadeau KC, Sayegh MH, Tilney NL: The role of the B7 costimulatory pathway in experimental cold ischemia/reperfusion injury. *J Clin Invest* 100: 1199–1203, 1997
27. Morooka T, Nishida E: Requirement of p38 mitogen-activated protein kinase for neuronal differentiation in PC12 cells. *J Biol Chem* 273: 24285–24288, 1998
28. Galbiati F, Volonte D, Engelman JA, Scherer PE, Lisanti MP: Targeted down-regulation of caveolin-3 is sufficient to inhibit myotube formation in differentiating C2C12 myoblasts: Transient activation of p38 mitogen-activated protein kinase is required for induction of caveolin-3 expression and subsequent myotube formation. *J Biol Chem* 274: 30315–30321, 1999
29. Houliston RA, Pearson JD, Wheeler-Jones CPD: Agonist-specific cross talk between ERKs and p38 MAPK regulates PGI2 synthesis in endothelium. *Am J Physiol Cell Physiol* 281: C1266–C1276, 2001
30. Hida M, Omori S, Awazu M: ERK and p38 MAP kinase are required for rat renal development. *Kidney Int* 61: 1252–1262, 2002
31. Yin T, Sandhu G, Wolfgang CD, Burrier A, Webb RL, Rigel DF, Hai T, Whelan J: Tissue-specific pattern of stress kinase activation in ischemic/reperfused heart and kidney. *J Biol Chem* 272: 19943–19950, 1997
32. Adhikary L, Chow F, Nikolic-Paterson DJ, Stambe C, Dowling J, Atkins RC, Tesch GH: Abnormal p38 mitogen-activated protein kinase signalling in human and experimental diabetic nephropathy. *Diabetologia* 47: 1210–1222, 2004
33. Sakai N, Wada T, Furuichi K, Iwata Y, Yoshimoto K, Kitagawa K, Kokubo S, Kobayashi M, Takeda S, Kida H, Kobayashi K, Mukaida N, Matsushima K, Yokoyama H: p38 MAPK phosphorylation and NF-kappaB activation in human crescentic glomerulonephritis. *Nephrol Dial Transplant* 17: 998–1004, 2002
34. Furuichi K, Wada T, Iwata Y, Sakai N, Yoshimoto K, Kobayashi KK, Mukaida N, Matsushima K, Yokoyama H: Administration of FR167653, a new anti-inflammatory compound, prevents renal ischaemia/reperfusion injury in mice. *Nephrol Dial Transplant* 17: 399–407, 2002
35. de Borst MH, Navis G, de Boer RA, Huitema S, Vis LM, van Gilst WH, van Goor H: Specific MAP-kinase blockade protects against renal damage in homozygous TGR (mRen2)27 rats. *Lab Invest* 83: 1761–1770, 2003
36. Aoudjit L, Stanciu M, Li H, Lemay S, Takano T: p38 mitogen-activated protein kinase protects glomerular epithelial cells from complement-mediated cell injury. *Am J Physiol Renal Physiol* 285: F765–F774, 2003
37. Schiffer M, Bitzer M, Roberts IS, Kopp JB, ten Dijke P,

Mundel P, Bottinger EP: Apoptosis in podocytes induced by TGF-beta and Smad7. *J Clin Invest* 108: 807–816, 2001
38. Kriz W, Gretz N, Lemley KV: Progression of glomerular diseases: Is the podocyte the culprit? *Kidney Int* 54: 687–697, 1998
39. Kang SW, Natarajan R, Shahed A, Nast CC, Mundel P, Kashtan C, Adler SG: Role of 12-lipoxygenase in the stimulation of p38 mitogen-activated protein kinase and collagen alpha5(IV) in experimental diabetic nephropathy and in glucose-stimulated podocytes. *J Am Soc Nephrol* 14: 3178–3187, 2003
40. Martineau LC, McVeigh LI, Jasmin BJ, Kennedy CRJ: p38 MAP kinase mediates mechanically induced COX-2 and PG EP4 receptor expression in podocytes: Implications for the actin cytoskeleton. *Am J Physiol Renal Physiol* 286: F693–F701, 2004
41. Iglesias-de la Cruz MC, Ziyadeh FN, Isono M, Kouahou M, Han DC, Kalluri R, Mundel P, Chen S: Effects of high glucose and TGF-beta1 on the expression of collagen IV and vascular endothelial growth factor in mouse podocytes. *Kidney Int* 62: 901–913, 2002
42. Chen S, Kasama Y, Lee JS, Jim B, Martin M, Ziyadeh FN: Podocyte-derived vascular endothelial growth factor mediates the stimulation of alpha3(IV) collagen production by transforming growth factor-beta1 in mouse podocytes. *Diabetes* 53: 2939–2949, 2004
43. Wang L, Kwak JH, Kim SI, He Y, Choi ME: Transforming growth factor-beta1 stimulates vascular endothelial growth factor 164 via mitogen-activated protein kinase kinase 3-p38alpha and p38delta mitogen-activated protein kinase-dependent pathway in murine mesangial cells. *J Biol Chem* 279: 33213–33219, 2004
44. Zhu T, Lobie PE: Janus kinase 2-dependent activation of p38 mitogen-activated protein kinase by growth hormone: Resultant transcriptional activation of ATF-2 and CHOP, cytoskeletal re-organization and mitogenesis. *J Biol Chem* 275: 2103–2114, 2000
45. Smoyer WE, Ransom RF: Hsp27 regulates podocyte cytoskeletal changes in an in vitro model of podocyte process retraction. *FASEB J* 16: 315–326, 2002
46. Mundel P, Shankland SJ: Podocyte biology and response to injury. *J Am Soc Nephrol* 13: 3005–3015, 2002
47. Remuzzi G, Bertani T: Pathophysiology of progressive nephropathies. *N Engl J Med* 339: 1448–1456, 1998
48. Morioka Y, Koike H, Ikezumi Y, Ito Y, Oyanagi A, Gejyo F, Shimizu F, Kawachi H: Podocyte injuries exacerbate mesangial proliferative glomerulonephritis. *Kidney Int* 60: 2192–2204, 2001
49. Pagtalunan ME, Miller PL, Jumping-Eagle S, Nelson RG, Myers BD, Rennke HG, Coplon NS, Sun L, Meyer TW: Podocyte loss and progressive glomerular injury in type II diabetes. *J Clin Invest* 99: 342–348, 1997
50. Lemley KV, Lafayette RA, Safai M, Derby G, Blouch K, Squarer A, Myers BD: Podocytopenia and disease severity in IgA nephropathy. *Kidney Int* 61: 1475–1485, 2002

Available online at www.sciencedirect.com

SCIENCE DIRECT®

Metabolism Clinical and Experimental 54 (2005) 1490–1498

Metabolism
Clinical and Experimental

www.elsevier.com/locate/metabol

Transgenic expression of mutant peroxisome proliferator–activated receptor γ in liver precipitates fasting–induced steatosis but protects against high-fat diet–induced steatosis in mice

Tomohiro Tanaka[a], Hiroaki Masuzaki[a,*], Ken Ebihara[a], Yoshihiro Ogawa[b], Shintaro Yasue[a], Hideo Yukioka[a,c], Hideki Chusho[a], Fumiko Miyanaga[a], Takashi Miyazawa[a], Muneya Fujimoto[a], Toru Kusakabe[a], Nozomi Kobayashi[a], Tatsuya Hayashi[d], Kiminori Hosoda[a], Kazuwa Nakao[a]

[a]*Department of Medicine and Clinical Science, Kyoto University Graduate School of Medicine, Kyoto, 606-8507, Japan*
[b]*Department of Molecular Medicine and Metabolism, Medical Research Institute, Tokyo Medical and Dental University, Tokyo, 101-0062, Japan*
[c]*Shionogi Discovery Research Laboratories, Shionogi and Co., Ltd., Osaka, 561-0825, Japan*
[d]*Department of Human Coexistence, Kyoto University Graduate School of Human and Environmental Studies, Kyoto, 606-8501, Japan*

Received 11 January 2005; accepted 10 May 2005

Abstract

Steatosis is one of the most common liver diseases and is associated with the metabolic syndrome. A line of evidence suggests that peroxisome proliferator–activated receptor (PPAR) α and PPARγ are involved in its pathogenesis. Hepatic overexpression of PPARγ1 in mice provokes steatosis, whereas liver-specific PPARγ disruption ameliorates steatosis in *ob/ob* mice, suggesting that hepatic PPARγ functions as an aggravator of steatosis. In contrast, PPARα-null mice are susceptible to steatosis because of reduced hepatic fatty acid oxidation. PPARγ with mutations in its C-terminal ligand-binding domain (L468A/E471A mutant PPARγ1) have been reported as a constitutive repressor of both PPARα and PPARγ activities in vitro. To elucidate the effect of cosuppression of PPARα and PPARγ on steatosis, we generated mutant PPARγ transgenic mice (Liver mt PPARγ Tg) under the control of liver-specific human serum amyloid P component promoter. In the liver of transgenic mice, PPARα and PPARγ agonist–induced augmentation of the expression of downstream target genes of PPARα and PPARγ, respectively, was significantly attenuated, suggesting PPARα and PPARγ cosuppression in vivo. Suppression of PPARα and PPARγ target genes was also observed in the fasted and high-fat–fed conditions. Liver mt PPARγ Tg were susceptible to fasting-induced steatosis while being protected against high-fat diet–induced steatosis. The opposite hepatic outcomes in Liver mt PPARγ Tg as a result of fasting and high-fat feeding may indicate distinct roles of PPARα and PPARγ in 2 different types of nutritionally provoked steatosis.

1. Introduction

Nonalcoholic fatty liver disease is now recognized as 1 of the common features of the metabolic syndrome [1-4], a cluster of visceral fat obesity, insulin resistance, dyslipidemia, and hypertension [5-7] and is a major contributor to obesity-related morbidity and mortality [1,2]. Intrahepatic lipid accumulation is responsible for systemic as well as hepatic insulin resistance [8,9].

The mechanisms underlying liver steatosis are complex and multifactorial [1,2,4,10,11]. However, a line of evidence suggests that peroxisome proliferator–activated receptor (PPAR) α and PPARγ, which regulate lipid metabolism [12], are involved in its pathogenesis [13-16]. Synthetic agonists for PPARα [17] and γ [18] have been widely used as lipid-lowering and antidiabetic agents, respectively, thus providing a therapeutic possibility for the treatment of steatosis by PPARα and/or PPARγ modulation [19,20]. PPARα is highly expressed in the liver and regulates a set of enzymes crucial for fatty acid oxidation [21,22]. PPARα-null mice exhibit fatty liver in elderly male animals [23], which is aggravated by either a high-fat diet (HFD) or

* Corresponding author. Tel.: +81 75 751 3172; fax: +81 75 771 9452.
E-mail address: hiroaki@kuhp.kyoto-u.ac.jp (H. Masuzaki).

0026-0495/$ – see front matter © 2005 Elsevier Inc. All rights reserved.
doi:10.1016/j.metabol.2005.05.015

starvation [14,24]. PPARγ is a key regulator of adipocyte differentiation and lipid storage [25,26]. Recent studies have revealed that PPARγ expression in the liver is augmented in murine steatosis [27-30]. Adenovirus-mediated overexpression of PPARγ in the liver provokes steatosis [31], whereas liver-specific disruption of PPARγ substantially ameliorates severe steatosis in *ob/ob* mice [15] and A-ZIP/F-1 mice, a murine model of lipoatrophic diabetes [16].

Mutations in the C-terminal (AF-2) domain of some nuclear receptors are known to generate proteins with a strong dominant negativity [32]. For example, L468A/E471A double-mutant of PPARγ1 has been reported to serve as a dominant-negative on PPARα and PPARγ1/PPARγ2 by recruiting and binding transcriptional corepressors, including the silencing mediator of retinoid and thyroid receptors and the nuclear corepressor [32].

To unravel the impact of L468A/E471A mutant PPARγ1 expression in the liver, we generated mutant PPARγ transgenic mice (Liver mt PPARγ Tg), in which the transgene (L468A/E471A mutant PPARγ1 cDNA) is exclusively expressed in the liver. The Liver mt PPARγ Tg were subjected to 2 distinct steatogenic stimuli (fasting and high-fat feeding) to examine the effect of mutant PPARγ on steatosis. In Liver mt PPARγ Tg, fasting-induced steatosis is aggravated, whereas HFD-induced steatosis is ameliorated, indicating that mutant PPARγ has distinct impacts on the pathophysiology of fasting- and HFD-induced steatosis.

2. Materials and methods

2.1. Plasmid construction, transfection, and luciferase assay

Full-length mouse PPARγ1 cDNA coding sequence was isolated from mouse epididymal adipose tissue total RNA by reverse transcriptase–polymerase chain reaction using Superscript II reverse transcriptase (Invitrogen, Carlsbad, Calif) and Takara ExTaq (Takara, Otsu, Japan). Three base-pair substitutions were introduced by site-directed mutagenesis that resulted in 2 missense mutations in the C-terminal (AF-2) domain of mouse PPARγ1 [32]. The resultant cDNA encoding L468A/E471A double-mutant PPARγ1 was cloned into the pCMX eukaryotic expression vector (a gift from Dr Kazuhiko Umesono, Nara Institute of Science and Technology, and Dr Ronald M. Evans, Salk Institute for Biological Studies) [33] to give pCMX-L468A/E471A PPARγ1 construct. Wild-type murine PPARα and PPARγ1 cDNA were also cloned into the pCMX vector and cotransfected with pCMX-L468A/E471A PPARγ1 and PPAR-responsive PPREx3-tk-LUC reporter [34] into human embryonic kidney (HEK) 293 cells using LipofectAMINE plus transfection kit (Invitrogen) [35] according to manufacturer's instructions. Cells were cultured for 36 hours in Dulbecco modified Eagle medium containing 10% bovine serum albumin [36]. Luciferase activity was measured by dual luminescence luciferase kit (Promega, Madison, Wis) as previously reported [36].

2.2. Animals

A fusion gene comprising the human serum amyloid P component promoter and mouse L468A/E471A PPARγ1 cDNA was designed so that the mutant PPARγ1 expression might be targeted to the liver [37,38]. The purified *Hind*III-*Xho*I fragment was microinjected into the pronucleus of fertilized C57BL/6N (Charles River Japan, Co, Tokyo, Japan) mouse eggs, and transgenic founder mice were generated [38]. The transgenic mice were identified by Southern blot analysis of the tail genomic DNA using cDNA fragment as a probe [38]. F2-3 heterozygous male mice were used for further experiments. Animals were individually housed and maintained on a chow diet (CE-1, 3.42 kcal/g [14.31 kJ/g], 11.6 kcal% [11.6 kJ%] fat, Japan CLEA, Tokyo, Japan) and on a 12-hour light cycle (light, 9:00 AM to 9:00 PM). All animals had ad libitum access to food and water unless otherwise mentioned. For drug administration, mice were fed power diet (CRF-1, Oriental Yeast Co, Ltd, Tokyo, Japan) containing 0.01% (wt/wt) pioglitazone (Takeda Chemical Industries, Osaka, Japan) for 3 weeks or 0.5% (wt/wt) bezafibrate (Kissei Pharmaceutical Co, Ltd, Nagano, Japan) for 6 days. Control mice were fed powder diet without drugs. The average daily food intake of powder diet–fed animals was 0.125 ± 0.006 g/g of body weight (n = 5) (no difference among mice fed control diet and diet containing pioglitazone or bezafibrate [n = 5]), which corresponds to ~12.5 mg/kg per day for pioglitazone and ~625 mg/kg per day for bezafibrate. For fasting experiment, 10-week-old mice were deprived of chow diet at 9:00 AM and were fasted for 72 hours, after which they were killed for the study. HFD (D12493, 5.24 kcal/g [21.92 kJ/g], 60 kcal% [60 kJ%] fat, Research Diets, New Brunswick, NJ) was initiated from 10 weeks of age and was continued for 19 weeks. Animals were anesthetized with diethyl ether before sampling. All animal experiments were performed according to National Institutes of Health guidelines and were approved by the Animal Research Committee, Graduate School of Medicine, Kyoto University.

2.3. Northern blot analysis and RNase protection assay

Liver total RNA was extracted using Trizol reagent (Invitrogen, Carlsbad, Calif) [38] and digested with RNase-free DNase (Qiagen, Hilden, Germany) according to manufacturer's instructions. Northern blot analysis was performed as previously described [38] using liver total RNA (40 μg per lane). RNase protection assay kit (Ambion, Austin, Tex) was used to hybridize liver and adipose tissue total RNA with radiolabeled RNA probe [39] generated from wild-type cDNA sequences spanning mutated nucleotides in L468A/E471A PPARγ1. To confirm the presence of transgene-derived mRNA, double-stranded RNA was digested with RNase A/T_1, electrophoresed on urea polyacrylamide gel, and subjected to autoradiography as previously described [39].

2.4. Liver Histology

Liver samples were fixed in 10% formalin neutral-buffered solution (Wako, Osaka, Japan) and embedded in paraffin wax, and 5-μm sections were cut and mounted on glass slides. After dehydration, the sections were stained with hematoxylin-eosin (H-E) [38] for histological examination.

2.5. Plasma assays and liver triglyceride content measurement

Plasma levels of alanine aminotransferase activity (Sigma, St Louis, Mo), triglyceride (Triglyceride-E test, Wako), non-esterified fatty acids (NEFA-C test, Wako), and insulin (Insulin ELISA kit, Morinaga, Yokohama, Japan) concentrations were determined according to manufacturer's instructions. Liver was homogenized in isopropyl alcohol and heptane, lipids were extracted [40], and the triglyceride content was determined by a kit using calorimetry (Triglyceride-E test, Wako).

2.6. Statistical analyses

Data were expressed as the mean ± SEM unless otherwise mentioned. Comparison between genotypes or animal groups was assessed by Student t test or analysis of variance, followed by Fisher probable least significant difference test where applicable.

3. Results

3.1. mRNA levels for PPARα and PPARγ were both augmented in fasting- and HFD-induced steatosis

Ten-week-old C57BL/6N wild-type male mice were fed ad libitum or food-deprived for 72 hours (n = 5). Another group of 10-week-old wild-type male mice was maintained either on a chow diet or HFD for 19 weeks (n = 5). The animals were killed, and the hepatic mRNA levels for PPARα and PPARγ were measured by Northern blot analysis. Hepatic expression of both PPARα and PPARγ was augmented in steatosis provoked by either fasting or HFD (Fig. 1).

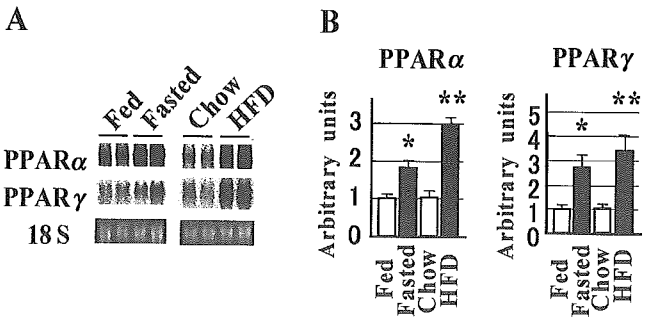

Fig. 1. Northern blot analysis of hepatic mRNA levels for PPARα and PPARγ in fasting-induced and high-fat diet–induced steatosis. Representative blots (A) and quantified data normalized by the intensity of ethidium bromide–stained 18S rRNA (B) (n = 5 for each group), *P < .05 vs Fed, **P < .05 vs Chow.

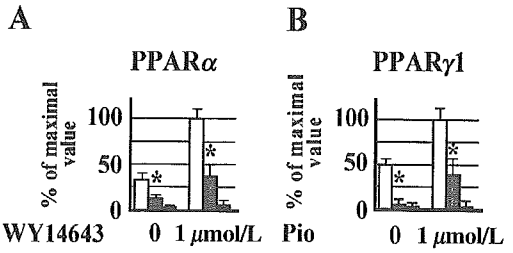

Fig. 2. PPRE-luciferase activity of PPARα (A) and PPARγ1 (B) (open bars) in the presence or absence of WY14643 (PPARα agonist) and Pio (pioglitazone: PPARγ agonist), respectively. Shaded bars represent the activity of PPARα (A) and PPARγ1 (B) with the cotransfection of L468A/E471A mutant PPARγγ1 cDNA. Dark bars represent the pCMX vector alone. Data are expressed as percent of maximal value (n = 6 for each bar), *P < .05 vs PPARα (A) or PPARγ1 (B).

3.2. Mutant PPARγ exhibits a dominant-negative effect on both PPARα and PPARγ in vitro

L468A/E471A double-mutant PPARγ1 has been reported to work in a dominant-negative fashion on PPARγ1 and γ2 in vitro [32]. Furthermore, authors of the report have shown that this mutant is capable of suppressing PPARα transcriptional activity [32]. We therefore hypothesized that the L468A/E471A mutant might be capable of suppressing the function of both PPARα and PPARγ. As expected, L468A/E471A mutant PPARγ1 repressed the transcriptional activities of PPARα and PPARγ1 when cotransfected into HEK293 cells (Fig. 2) (n = 6 for each column). A dominant-negative effect was observed in both the presence and absence of each specific agonist for PPARα and PPARγ (Fig. 2). We then used L468A/E471A mutant PPARγ1 to suppress PPARα and γ activities in the liver in vivo.

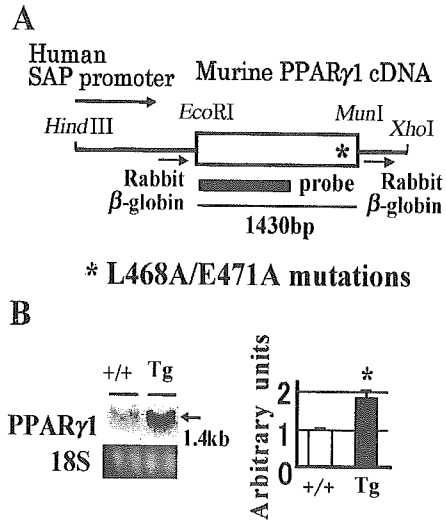

Fig. 3. DNA construct for the generation of Liver mt PPARγ Tg (A). The position of the L468A/E471A mutations in the construct is indicated by an asterisk. B, Northern blot analysis of hepatic mRNA level for PPARγ in wild-type mice (+/+) and Liver mt PPARγ Tg (Tg). The DNA probe used for Northern blot analysis is indicated in A. Representative blot and quantified data normalized by the 18S rRNA expression level are shown (n = 5 for each genotype), *P < .05 vs +/+.